Mathematical Methods of Operations Research
https://doi.org/10.1007/s00186-024-00875-y

ORIGINAL ARTICLE

Inverse demand tracking in transportation networks

Simone Göttlich[1] · **Patrick Mehlitz**[2] · **Thomas Schillinger**[1]

Received: 14 July 2023 / Revised: 9 August 2024 / Accepted: 15 August 2024

Abstract
This paper deals with the reconstruction of the desired demand in an optimal control problem, stated over a tree-shaped transportation network which is governed by a linear hyperbolic conservation law. As desired demands typically undergo fluctuations due to seasonality or unexpected events making short-term adjustments necessary, such an approach can exemplary be used for forecasting from past data. We suggest to model this problem as a so-called inverse optimal control problem, i.e., a hierarchical optimization problem whose inner problem is the optimal control problem and whose outer problem is the reconstruction problem. In order to guarantee the existence of solutions in the function space framework, the hyperbolic conservation law is interpreted in weak sense allowing for control functions in Lebesgue spaces. For the computational treatment of the model, we transfer the hierarchical problem into a nonsmooth single-level one by plugging the uniquely determined solution of the inner optimal control problem into the outer reconstruction problem before applying techniques from nonsmooth optimization. Some numerical experiments are presented to visualize various features of the model including different types of noise in the demand and strategies of how to observe the network in order to obtain good reconstructions of the desired demand.

Keywords Inverse optimal control · Linear hyperbolic conservation laws · Transportation networks

Mathematics Subject Classification 49J20 · 65M32 · 90C33 · 90C35

✉ Simone Göttlich
goettlich@uni-mannheim.de

Patrick Mehlitz
mehlitz@uni-marburg.de

Thomas Schillinger
schillinger@uni-mannheim.de

[1] School of Business Informatics and Mathematics, University of Mannheim, 68159 Mannheim, Germany

[2] Department of Mathematics and Computer Science, Philipps-Universität Marburg, 35032 Marburg, Germany

Published online: 05 October 2024

1 Introduction

Flow problems over energy and supply networks model a broad range of interesting applications, see (Bressan et al. 2014) for a survey. In this paper, we investigate transportation networks of tree shape where the flow on edges is modeled, for simplicity, via (linear) hyperbolic conservation laws, as typically used for electric transmission lines (Göttlich et al. 2016), heating networks (Rein et al. 2020), or networks of gas pipelines (Banda et al. 2006; Gugat et al. 2018). A control function is used to model the inflow at some source vertex, and the aim of optimization is to choose this function in such a way that certain desired demands at the sinks of the network are tracked as close as possible. As mentioned in some recent contributions, see (Göttlich et al. 2019; Göttlich and Schillinger 2022a, b), these desirable demands are subject to perturbations, noise, or other sources of stochasticity. In the aforementioned papers, this issue has been faced by modeling the problem as a stochastic optimal control problem which is influenced by randomness via appropriately chosen stochastic processes.

In this paper, we are concerned with related phenomena. Let us consider the following practically relevant situation. There exists a company (C2) which appoints a second company (C1) to deliver a certain amount of electricity/heat/gas at the demand vertices over time by inserting the requested product at the source of the network over time. In this regard, C1 has to solve the optimal control problem mentioned above. We now enrich the considered situation by assuming that there is a network operator (NO), different from C1 and C2, which partially observes the flow along the network and, depending on this, charges C1 and C2 to pay some tax for employing the network. As outlined above, the desired demands requested by C2 are subject to stochastic influences and, additionally, may vary due to a seasonal behavior. From past data, NO now wants to forecast the desired demand of C2 and the associated actions of C1, exemplary for fixing taxes to plan future income. Typically, NO is not aware of the desired demand as he only observes the actual network flow along some but, most likely, not all edges of the network (as it might be expensive to equip the overall network with sensors or to run them on each edge over all time). Furthermore, the forecasting model should be capable of recognizing seasonal behavior of the desired demands as it is exemplarily presented for an electricity market in Coskun and Korn (2021).

In order to model this situation, we consider it from the viewpoint of inverse optimal control, i.e., we aim to identify parameters in an optimal control problem (and not only in a dynamical system). Here, the optimal control problem of interest is the aforementioned network flow problem, and the appearing desired demand plays the role of this parameter. We assume that we are given observed (but, most likely, noisy) pairs of optimal inflow and optimal network flow, and aim to reconstruct the desired demands which are modeled as a convex combination of given ansatz functions. It is, thus, our goal to find the associated weight parameters which characterize a suitable standard (periodically emerging) choice for the desired demand. As we are interested in the robustness of our approach, we consider additional perturbations in the model and study different types of temporal restrictions in the observation of the network to evaluate whether these are sufficient for good forecasting.

Naturally, the model of interest is a hierarchical optimization problem with two decision levels. Coming back to our exemplary situation from above, at the outer

(or upper-level) problem, the NO is in position to partially observe the network and chooses certain weights, which then give a tangible desired demand. At the inner (or lower-level) problem, C1 now can solve the network flow problem. Along those parts of the network, which are observed by NO, the latter can compare the past data and the real-time data obtained from the inner problem for this particular choice of the weight parameters. Noting that this decision order leads to a well-posed problem, NO aims to choose the weight parameters in such a way that past data and real-time data match as good as possible. As our model has two decision levels, it is a so-called bilevel optimization problem.

For more than 50 years, bilevel optimization is a major field of research in mathematical programming due to numerous underlying applications e.g. in data science, economy, finance, machine learning, or natural sciences, see (Bard 1998; Dempe 2002; Shimizu et al. 1997) for an introduction and Dempe (2020) for a recent survey which presents an overview of contributions in this area. Recently, bilevel optimization turned out to be of particular interest in the context of transportation or energy networks, see e.g. Dempe et al. (2015). This also includes the rapidly growing field of hierarchical control, see e.g. Mehlitz and Wachsmuth (2020) for an overview, and, particularly, so-called inverse optimal control already mentioned earlier, see (Hinze et al. 2009; Tröltzsch 2010; Troutman 1996; Vinter 2010) for an introduction to the topic of optimal control. Inverse control possesses several interesting applications e.g. in the context of human locomotion, see (Albrecht et al. 2012; Albrecht and Ulbrich 2017; Albrecht et al. 2010; Mombaur et al. 2010). The theory on inverse optimal control including ordinary and partial differential equations addresses the existence of solutions, optimality conditions, and solution algorithms, see e.g. (Dempe et al. 2019; Friedemann et al. 2023; Harder and Wachsmuth 2019; Hatz et al. 2012; Holler et al. 2018; Suryan et al. 2016) and is developing fast. In abstract bilevel optimization, two decision makers, a leader and a follower, need to choose variables in order to minimize their associated cost function which also depends on the variables of the other decision maker, respectively. More precisely, the leader chooses his variables first which are handed over to the follower who now can solve his optimization problem (which is parametric in the leader's variable) to global optimality. The solutions are then given to the leader, who now can evaluate his objective. Often, one assumes that leader and follower cooperate in order to optimize the leader's objective, and this procedure is referred to as the optimistic approach to the problem, see (Zemkoho 2016) for an overview of other approaches avoiding ill-posedness in bilevel optimization. The leader's and follower's problem are often referred to as upper- and lower-level problem, respectively. As the follower has to determine globally optimal solutions of his problem by nature of bilevel optimization, one typically requires that the lower-level problem is convex in the follower's variable in order to circumvent issues related to nonconvex global optimization at the lower-level stage.

We start our investigations by modeling the problem of interest as an inverse control problem in Sect. 2. Therefore, we first study the existence of solutions for linear hyperbolic conservation laws in a function space which is suitable for optimal control before setting up the lower- and upper-level problem consecutively. Furthermore, we demonstrate that the resulting optimization problem possesses an optimal solution in the function space setting we are investigating. In Sect. 3, we address the computa-

tional treatment of the model. Section 3.1 describes our approach to the numerical solution of the problem. As it is analytically possible to compute the network flow associated with the input, we are in position to distill a state-reduced version of the parametric optimal control problem. The associated solution operator, which, at least in pointwise fashion, can similarly be computed analytically due to the nice structure of the problem, turns out to be a nonsmooth single-valued mapping. Plugging the latter into the superordinate reconstruction problem and performing a suitable discretization, we end up with a nonsmooth optimization which we solve with the aid of MATLAB's `patternsearch` solver in default mode. The general set-up of our computational experiments is carved out in Sect. 3.2. Numerical results are presented in Sect. 3.3 in order to visualize the effectiveness and several different features of the approach. Particular focus is laid on the robustness of the model with respect to additional uncertainties, restricted observation options, and the presence of additional inflow constraints. Some concluding remarks close the paper in Sect. 4.

2 The model problem

In this section, we set up the model of our interest. First, we discuss the particular shape of the lower-level parametric optimal control problem in Sect. 2.1. Therefore, we first present the underlying network dynamics and discuss regularity features of associated solutions. Second, the lower-level objective function is constructed, and solvability of the overall lower-level problem is discussed. In Sect. 2.2, we derive the superordinate upper-level problem and demonstrate that it possesses an optimal solution in the function space setting.

2.1 The lower-level problem

In this subsection, we are concerned with the derivation and analysis of the lower-level optimal control problem. To start, we state the lower-level dynamics and discuss existence and uniqueness of solutions associated with this system. Afterwards, we set up the (parametric) lower-level problem, show that, for each set of parameters, it possesses a unique solution, and investigate properties of the associated solution operator.

2.1.1 Setting up the network and network dynamics

We consider a directed graph $G = (V, E)$ which is a tree (in the sense that whenever the directed edges are interpreted as undirected, then the resulting graph would be free of cycles). Let us use the notation $V := \{v_0, \ldots, v_n\}$ and note that $|E| = n$ by nature of trees. Some more details on G and the notation we are going to exploit are discussed below.

- The uniquely determined source vertex of the network G is $v_0 \in V$. Furthermore, we assume that v_0 is a leaf of G, i.e., there is only one edge which leaves v_0, and the vertex at its end will be denoted by v_1.

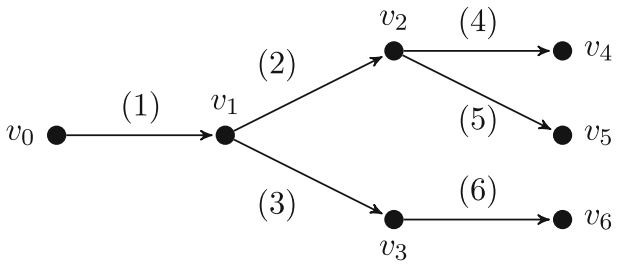

Fig. 1 An exemplary network with $V_D = \{v_4, v_5, v_6\}$, $V_I = \{v_1, v_2, v_3\}$, $E^+(2) = \{(4), (5)\}$, and $E_D = \{(4), (5), (6)\}$

- In $V_D \subset V$, we collect all vertices which possess no outgoing edges. These are the demand vertices.
- All remaining intermediate (or inner) vertices of the network are collected in the set $V_I := V \setminus (V_D \cup \{v_0\})$.
- For $v_i \in V \setminus \{v_0\}$, we identify the uniquely determined edge which ends at v_i by (i).
- The set $E^+(i)$ is used to denote the set of all edges starting at vertex v_i. Furthermore, we use $E_D := \{(i) \in E \mid v_i \in V_D\}$ to denote the set of edges that end at a demand vertex. Clearly, $|E_D| = |V_D|$.

We visualize the above notation in Fig. 1. For the theory of this paper, it is not mandatory that the vertex v_0 possesses just one outgoing edge. One can interpret v_0 as an upstream supersource. Besides, this additional assumption simplifies the notation because we can abstain from the introduction of distribution parameters at the inflow vertex later on.

At the source v_0, the injection of flow over time $\mathcal{T} := (0, T)$, where $T > 0$ is the final time, is modeled by the control variable $u : \mathcal{T} \to \mathbb{R}$ which has to be chosen from an appropriate function space.

The flow over (i) at time $t \in \mathcal{T}$ at the spatial coordinate $x \in \Omega$ will be denoted by $z^{(i)}(t, x)$. Here, we assume that $\Omega := (0, \omega)$ is a bounded real interval. The density has to obey the linear hyperbolic conservation law

$$z_t^{(i)}(t, x) + \lambda^{(i)} z_x^{(i)}(t, x) = 0, \qquad \text{a.e. on } \mathcal{T} \times \Omega,\ (i) \in E, \tag{2.1a}$$

$$z^{(i)}(0, x) = 0, \qquad \text{a.e. on } \Omega,\ (i) \in E, \tag{2.1b}$$

$$\lambda^{(1)} z^{(1)}(t, 0) = u(t), \qquad \text{a.e. on } \mathcal{T}, \tag{2.1c}$$

$$\lambda^{(k)} z^{(k)}(t, 0) = \alpha_{i,k} \lambda^{(i)} z^{(i)}(t, \omega), \qquad \text{a.e. on } \mathcal{T},\ v_i \in V_I,\ (k) \in E^+(i). \tag{2.1d}$$

Particularly, the flux functions of the conservation law are of linear structure. For each $i \in \{1, \ldots, n\}$, $\lambda^{(i)} > 0$ is a given constant. Above, for each $v_i \in V_I$ and $(k) \in E^+(i)$, $\alpha_{i,k} > 0$ is a constant such that $\sum_{(k) \in E^+(i)} \alpha_{i,k} = 1$ holds, i.e., the coefficients $\alpha_{i,k}$ model how the flow splits at vertex v_i into the flows along the edges from $E^+(i)$. This way, (2.1d) conserves the flow. We note that the theory can be extended to more general situations. Exemplary, standard linear damping terms of type $\mu^{(i)} z^{(i)}(t, x)$

can be incorporated in (2.1a) for real constants $\mu^{(i)} > 0$ for each $(i) \in E$ without any problem. Under additional assumptions, the coefficients $\lambda^{(i)}$ and $\mu^{(i)}$ may also depend on time. Without loss of generality one could choose $\omega := 1$. However, in order to clearly distinguish between temporal and spatial variables in notation, we stick to the seemingly more general situation where $\omega > 0$ is arbitrary. Furthermore, the findings in this paper extend to connected networks without cycles, but apart from a more difficult notation, which also allows for vertices where flows are merged, we do not believe that such a model comes along with a significantly different theory. We, thus, concentrate on tree-shaped networks.

2.1.2 Discussion of the hyperbolic conservation law

Let us first review a classical existence result for the linear hyperbolic conservation law (2.1). Therefore, we define a suitable control space by

$$C^1_{00}(\overline{\mathcal{T}}) := \left\{ u \in C^1(\overline{\mathcal{T}}) \,|\, u(0) = 0,\ u'(0) = 0 \right\}.$$

We equip $C^1_{00}(\overline{\mathcal{T}})$ with the classical C^1-norm, and note that this space is a closed subspace of $C^1(\overline{\mathcal{T}})$. The proof of the following result, which is based on the method of characteristics, can be distilled from Bressan (Bressan 2000, Section 3.1, Theorems 3.4 and 3.6) under the condition that we only consider positive velocities on the network and, thus, all waves are moving with positive speed.

Proposition 2.1 *For each $u \in C^1_{00}(\overline{\mathcal{T}})$, the hyperbolic conservation law (2.1) possesses a unique solution $z := (z^{(1)}, \dots, z^{(n)}) \in C^1(\overline{\mathcal{T} \times \Omega}, \mathbb{R}^n)$. The latter is explicitly given by*

$$\forall (t,x) \in \overline{\mathcal{T} \times \Omega}: \quad z^{(1)}(t,x) = \begin{cases} \frac{1}{\lambda^{(1)}} u(t - x/\lambda^{(1)}) & t - x/\lambda^{(1)} > 0, \\ 0 & t - x/\lambda^{(1)} \leq 0 \end{cases} \tag{2.2}$$

on edge (1), and for each $i \in \{1, \dots, n\}$ such that $v_i \in V_I$ and $(k) \in E^+(i)$, we find

$$\forall (t,x) \in \overline{\mathcal{T} \times \Omega}: \quad z^{(k)}(t,x) = \begin{cases} \alpha_{i,k} \frac{\lambda^{(i)}}{\lambda^{(k)}} z^{(i)}(t - x/\lambda^{(k)}, \omega) & t - x/\lambda^{(k)} > 0, \\ 0 & t - x/\lambda^{(k)} \leq 0. \end{cases} \tag{2.3}$$

Additionally, there is a constant $\kappa > 0$, not depending on u, such that $\|z\|_{C^1(\overline{\mathcal{T} \times \Omega}, \mathbb{R}^n)} \leq \kappa \|u\|_{C^1(\overline{\mathcal{T}})}$.

Let us note that formula (2.3) can be used recursively to determine the solution along all edges of the network. Indeed, based on (2.2), the solution along all arcs from $E^+(1)$ can be computed. Next, using (2.3), it is possible to determine the flow along all edges starting in those vertices which are the end vertex of some edge in $E^+(1)$. Repeating this procedure, one can iterate through the whole network.

Clearly, Proposition 2.1 justifies to introduce a map from $C^1_{00}(\overline{\mathcal{T}})$ to $C^1(\overline{\mathcal{T} \times \Omega}, \mathbb{R}^n)$ which assigns to each control function from $C^1_{00}(\overline{\mathcal{T}})$ the associated uniquely determined solution of (2.1). This mapping is a linear operator which is continuous by Proposition 2.1.

Since we are interested in the optimal control of the system (2.1), working with the control space $C^1_{00}(\overline{\mathcal{T}})$ induces some inherent difficulties. First, this space is nonreflexive, i.e., to show the existence of optimal solutions for optimization problems over (2.1) and the superordinate inverse optimal control problem, which we state in Sect. 2.2, would be challenging. Second, the dual of this space, which naturally arises when using the adjoint approach for the derivation of optimality conditions, is large and difficult to handle numerically. It is, thus, a reasonable task to reconsider (2.1) from the viewpoint of control functions $u \in L^2(\mathcal{T})$. Besides, this choice allows for discontinuous controls which can be exploited to model switches in the inflow. Observe that (2.1) does not need to possess a classical solution in the sense of Proposition 2.1 anymore whenever the control function is not continuously differentiable. To proceed, we follow (Keimer 2014, Section 2.2), see (Gugat et al. 2015, Section 2) as well, to introduce a suitable weak formulation of (2.1) as stated below. First, for the state $z^{(1)}$, we demand

$$\int_{\mathcal{T}_\tau} \int_\Omega z^{(1)}(t,x)(\varphi_t(t,x) + \lambda^{(1)}\varphi_x(t,x))\mathrm{d}x\mathrm{d}t = -\int_{\mathcal{T}_\tau} u(t)\varphi(t,0)\mathrm{d}t \quad \forall \varphi \in W_\tau \tag{2.4}$$

for all $\tau \in \overline{\mathcal{T}}$, where $\mathcal{T}_\tau := (0,\tau)$ and

$$W_\tau := \left\{ \varphi \in C^1(\overline{\mathcal{T}_\tau \times \Omega}) \;\middle|\; \begin{array}{ll} \varphi(\cdot,\omega) = 0 & \text{on } \overline{\mathcal{T}_\tau} \\ \varphi(\tau,\cdot) = 0 & \text{on } \overline{\Omega} \end{array} \right\}$$

is the space of test functions. Similarly as above, we demand

$$\int_{\mathcal{T}_\tau} \int_\Omega z^{(k)}(t,x)(\varphi_t(t,x) + \lambda^{(k)}\varphi_x(t,x))\mathrm{d}x\mathrm{d}t = -\alpha_{i,k}\lambda^{(i)} \int_{\mathcal{T}_\tau} z^{(i)}(t,\omega)\varphi(t,0)\mathrm{d}t \quad \forall \varphi \in W_\tau \tag{2.5}$$

for all $\tau \in \overline{\mathcal{T}}$, $v_i \in V_I$, and $(k) \in E^+(i)$. A function $z \in C(\overline{\Omega}, L^2(\mathcal{T}, \mathbb{R}^n))$ satisfying these requirements is referred to as a weak solution of the hyperbolic conservation law (2.1). Recall that the function space $C(\overline{\Omega}, L^2(\mathcal{T}, \mathbb{R}^n))$ comprises all functions $z\colon \mathcal{T} \times \overline{\Omega} \to \mathbb{R}^n$ such that, for each $x \in \overline{\Omega}$, $z(\cdot,x)$ belongs to $L^2(\mathcal{T}, \mathbb{R}^n)$, and $\overline{\Omega} \ni x \to z(\cdot,x) \in L^2(\mathcal{T}, \mathbb{R}^n)$ is continuous. Let us emphasize that the boundary conditions (2.1b), (2.1c) are incorporated in this alternative formulation of the dynamics also in weak sense only (by definition of the space W_τ) since pointwise considerations are meaningless in Lebesgue spaces.

The following result shows that the (classical) solution characterized in Proposition 2.1 (with controls chosen from $C^1_{00}(\overline{\mathcal{T}})$) also provides the uniquely determined weak solution of the hyperbolic conservation law (2.1) if the control is chosen from $L^2(\mathcal{T})$.

Proposition 2.2 *For each $u \in L^2(\mathcal{T})$, the function $z := (z^{(1)}, \dots, z^{(n)}) \in C(\overline{\Omega}, L^2(\mathcal{T}, \mathbb{R}^n))$ characterized via (2.2), (2.3) is the uniquely determined weak solution of the hyperbolic conservation law (2.1). Additionally, there is a constant $\kappa > 0$, not depending on u, such that $\|z\|_{C(\overline{\Omega}, L^2(\mathcal{T}, \mathbb{R}^n))} \leq \kappa \, \|u\|_{L^2(\mathcal{T})}$.*

Proof Let us start to show that $z^{(1)}$ given in (2.2) satisfies (2.4) for each $\tau \in \overline{\mathcal{T}}$ and given $u \in L^2(\mathcal{T})$. Therefore, we introduce a function $\bar{u} \in L^2((-\omega/\lambda^{(1)}, T))$ by

$$\forall t \in (-\omega/\lambda^{(1)}, T): \quad \bar{u}(t) := \begin{cases} u(t) & t > 0, \\ 0 & t \leq 0. \end{cases}$$

Using a coordinate transformation with respect to the new domain

$$\Xi_\tau := \{(s, x) \in \mathbb{R}^2 \,|\, x \in \Omega,\ s \in (-x/\lambda^{(1)}, \tau - x/\lambda^{(1)})\},$$

we find, for each $\varphi \in W_\tau$ and $\bar{\varphi}(s, x) := \varphi(s + x/\lambda^{(1)}, x)$ for all $(s, x) \in \Xi_\tau$, the identities

$$\begin{aligned}
&\int_{\mathcal{T}_\tau} \int_\Omega z^{(1)}(t, x)(\varphi_t(t, x) + \lambda^{(1)} \varphi_x(t, x)) \mathrm{d}x \mathrm{d}t \\
&= \frac{1}{\lambda^{(1)}} \int_{\mathcal{T}_\tau} \int_\Omega \bar{u}(t - x/\lambda^{(1)})(\varphi_t(t, x) + \lambda^{(1)} \varphi_x(t, x)) \mathrm{d}x \mathrm{d}t \\
&= \iint_{\Xi_\tau} \bar{u}(s) \bar{\varphi}_x(s, x) \, \mathrm{d}(s, x) \\
&= \int_{-\omega/\lambda^{(1)}}^{\tau} \int_{\max(0, -\lambda^{(1)} s)}^{\min(\omega, \lambda^{(1)}(\tau - s))} \bar{u}(s) \bar{\varphi}_x(s, x) \mathrm{d}x \mathrm{d}s \\
&= \int_0^\tau u(s) \int_0^{\min(\omega, \lambda^{(1)}(\tau - s))} \bar{\varphi}_x(s, x) \mathrm{d}x \mathrm{d}s \\
&= \int_0^\tau u(s)(\bar{\varphi}(s, \min(\omega, \lambda^{(1)}(\tau - s))) - \bar{\varphi}(s, 0)) \mathrm{d}s \\
&= -\int_{\mathcal{T}_\tau} u(s) \varphi(s, 0) \mathrm{d}s.
\end{aligned}$$

Above, we used the fact that the determinant of the Jacobian associated with the chosen coordinate transform is 1, the fundamental theorem of calculus, and

$$\bar{\varphi}(s, \min(\omega, \lambda^{(1)}(\tau - s))) = \begin{cases} \varphi(\tau, \lambda^{(1)}(\tau - s)) = 0 & \lambda^{(1)}(\tau - s) < \omega, \\ \varphi(s + \omega/\lambda^{(1)}, \omega) = 0 & \lambda^{(1)}(\tau - s) \geq \omega, \end{cases}$$

which holds by definition of the space W_τ of test functions. Thus, the function from (2.2) solves (2.4).

Next, we will verify $z^{(1)} \in C(\overline{\Omega}, L^2(\mathcal{T}))$. By definition of $z^{(1)}$, $z^{(1)}(\cdot, x) \in L^2(\mathcal{T})$ is obvious for each $x \in \overline{\Omega}$. Let us pick $x_1, x_2 \in \overline{\Omega}$ such that, without loss of generality, $x_1 < x_2$. Then we have

$$\begin{aligned}
&\|z^{(1)}(\cdot, x_1) - z^{(1)}(\cdot, x_2)\|^2_{L^2(\mathcal{T})} \\
&\quad = \frac{1}{(\lambda^{(1)})^2} \int_0^T \left(\bar{u}(t - x_1/\lambda^{(1)}) - \bar{u}(t - x_2/\lambda^{(1)})\right)^2 \mathrm{d}t \\
&\quad = \frac{1}{(\lambda^{(1)})^2} \left(\int_{x_1/\lambda^{(1)}}^{x_2/\lambda^{(1)}} u^2(t - x_1/\lambda^{(1)}) \mathrm{d}t + \int_{x_2/\lambda^{(1)}}^{T} \left(u(t - x_1/\lambda^{(1)}) - u(t - x_2/\lambda^{(1)})\right)^2 \mathrm{d}t \right).
\end{aligned}$$

As $|x_1 - x_2| \to 0$, the first of these integrals trivially tends to 0, and one can exploit similar arguments as used to prove (Dobrowolski 2006, Theorems 4.20, 4.21) in order to verify that the second integral tends to 0 as well. Hence, $x \mapsto z^{(1)}(\cdot, x)$ is continuous on $\overline{\Omega}$, i.e., $z^{(1)} \in C(\overline{\Omega}, L^2(\mathcal{T}))$. Let us also note that

$$\begin{aligned}
\|z^{(1)}\|^2_{C(\overline{\Omega}, L^2(\mathcal{T}))} &= \max_{x \in [0,\omega]} \|z^{(1)}(\cdot, x)\|^2_{L^2(\mathcal{T})} \\
&= \frac{1}{(\lambda^{(1)})^2} \max_{x \in [0,\omega]} \int_0^T \bar{u}^2(t - x/\lambda^{(1)}) \mathrm{d}t \\
&= \frac{1}{(\lambda^{(1)})^2} \max_{x \in [0,\omega]} \int_0^{\max(0, T - x/\lambda^{(1)})} u^2(s) \mathrm{d}s \\
&\leq \frac{1}{(\lambda^{(1)})^2} \max_{x \in [0,\omega]} \int_0^T u^2(s) \mathrm{d}s = \frac{1}{(\lambda^{(1)})^2} \|u\|^2_{L^2(\mathcal{T})},
\end{aligned}$$

which gives

$$\|z^{(1)}\|_{C(\overline{\Omega}, L^2(\mathcal{T}))} \leq (\lambda^{(1)})^{-1} \|u\|_{L^2(\mathcal{T})}.$$

The above arguments can be repeated in order to show that, for each $i \in \{1, \ldots, n\}$ such that $v_i \in V_I$ and $(k) \in E^+(i)$, the function $z^{(k)}$ characterized in (2.3) satisfies (2.5) for each $\tau \in \overline{\mathcal{T}}$, belongs to $C(\overline{\Omega}, L^2(\mathcal{T}))$, and obeys the estimate

$$\|z^{(k)}\|_{C(\overline{\Omega}, L^2(\mathcal{T}))} \leq \frac{\lambda^{(i)}}{\lambda^{(k)}} \|z^{(i)}\|_{C(\overline{\Omega}, L^2(\mathcal{T}))}.$$

By iteration through the whole network, we obtain that the considered function z is a weak solution of the hyperbolic conservation law (2.1) which belongs to $C(\overline{\Omega}, L^2(\mathcal{T}, \mathbb{R}^n))$. Finally, uniqueness of the weak solution follows from Keimer (2014, Theorem 3.1.1). □

Proposition 2.2 motivates the following definition.

Definition 2.3 Let $S\colon L^2(\mathcal{T}) \to C(\overline{\Omega}, L^2(\mathcal{T}, \mathbb{R}^n))$ be the operator which assigns to each $u \in L^2(\mathcal{T})$ the uniquely determined weak solution of the hyperbolic conservation law (2.1) which has been discussed in Proposition 2.2. For each $u \in L^2(\mathcal{T})$, we make use of the notation $S^{(i)}(u)$ and $S^{(i)}_\omega(u)$ to address the i-th component function of $S(u)$ and the function $S^{(i)}(u)(\cdot, \omega) \in L^2(\mathcal{T})$ for all $i \in \{1, \dots, n\}$, respectively.

The operator S defined above encapsulates all the information provided by (2.1) and later on allows us to state all optimization problems of interest in compact, state-reduced form.

Remark 2.4 Due to Proposition 2.2, the operator S is linear and continuous. Furthermore, for each $i \in \{1, \dots, n\}$, $S^{(i)}\colon L^2(\mathcal{T}) \to C(\overline{\Omega}, L^2(\mathcal{T}))$ and $S^{(i)}_\omega\colon L^2(\mathcal{T}) \to L^2(\mathcal{T})$ are linear and continuous operators.

Let us note that an alternative approach to access the analysis of the linear hyperbolic conservation law (2.1) is given via semigroup theory, see e.g. Sikolya (2004).

2.1.3 The lower-level problem and its solution operator

Now, we are ready to formulate the optimal control problem of interest. In general, the control function $u \in L^2(\mathcal{T})$ has to be chosen from a certain set of feasible controls such that a given demand is tracked while the control effort is minimal. This is achieved by minimizing the expression

$$f(u, \beta) := \frac{1}{2} \sum_{(i) \in E_D} \left\| S^{(i)}_\omega(u) - \sum\nolimits_{\ell=1}^{m} \beta^{(i)}_\ell D^{(i)}_\ell \right\|^2_{L^2(\mathcal{T})} + \frac{\sigma}{2} \|u\|^2_{L^2(\mathcal{T})} \tag{2.6}$$

with respect to $u \in U_{\mathrm{ad}} \subset L^2(\mathcal{T})$, where

$$U_{\mathrm{ad}} := \{u \in L^2(\mathcal{T}) \mid u_{\mathrm{a}}(t) \le u(t) \le u_{\mathrm{b}}(t) \text{ a.e. on } \mathcal{T}\} \tag{2.7}$$

is a standard box-constrained set induced by given measurable functions $u_{\mathrm{a}}\colon \mathcal{T} \to \{-\infty\} \cup \mathbb{R}$ and $u_{\mathrm{b}}\colon \mathcal{T} \to \mathbb{R} \cup \{\infty\}$, and we assume that U_{ad} is nonempty. In (2.6), $m \in \mathbb{N}$ such that $m \ge 2$ is a fixed natural number which does not depend on (i) for simplicity. Recall that $S(u)$ is used to represent the (weak) solution of (2.1) which we discussed in Sect. 2.1.2, $S^{(i)}(u)$ is the component of $S(u)$ which is associated with the edge $(i) \in E$, $i \in \{1, \dots, n\}$, and $S^{(i)}_\omega(u) \in L^2(\mathcal{T})$ is obtained from $S^{(i)}(u)$ by fixing the spatial variable to $x := \omega$, see Definition 2.3 as well. When controlling network flows, one typically tries to track the demand only by means of the outflow at the demand vertices over time, and this is reflected by definition of (2.6). The appearing regularization term aims to minimize the control effort and, in parallel, guarantees uniqueness of lower-level solutions as we will see later on, see Proposition 2.5 below.

In (2.6), for each $(i) \in E_D$, $D^{(i)}_1, \dots, D^{(i)}_m \in L^2(\mathcal{T})$ are typical demand profiles, i.e., suitable ansatz functions modeling the outflow at demand vertices over time. Furthermore, $\sigma > 0$ is a regularization parameter. The weights $\beta^{(i)} \in \Lambda^m$, where

$$\Lambda^m := \{b \in \mathbb{R}^m \,\big|\, b \ge 0,\ \sum\nolimits_{\ell=1}^{m} b_\ell = 1\} \tag{2.8}$$

denotes the standard simplex in $\mathbb{R}^m$, are, at the lower-level stage, fixed and shall be reconstructed from measurements in a superordinate optimization problem, see Sect. 2.2. For fixed $(i) \in E_D$, $\sum_{\ell=1}^m \beta_\ell^{(i)} D_\ell^{(i)}$ plays the role of the desired demand, i.e., the outflow at demand vertex v_i over time we are seeking. In this regard and by definition of Λ^m, $D_1^{(i)}, \dots, D_m^{(i)}$ play the role of extreme cases for the desired demand as $\sum_{\ell=1}^m \beta_\ell^{(i)} D_\ell^{(i)}$ is a convex combination of these functions. If $D_1^{(i)}, \dots, D_m^{(i)}$ are interpreted merely as basis functions of a suitable finite-dimensional subspace of $L^2(\mathcal{T})$, where the desired demand has to be chosen from, then the weights $\beta^{(i)}$ can be taken as arbitrary vectors from $\mathbb{R}^m$, resulting in an easier superordinate reconstruction problem. In (2.6), we used $\beta := (\beta^{(i)})_{(i)\in E_D} \in (\mathbb{R}^m)^{|V_D|}$ for brevity of notation.

We investigate the lower-level optimal control problem

$$\min_u \{ f(u, \beta) \mid u \in U_{\text{ad}} \}. \tag{LL(β)}$$

Here, $f\colon L^2(\mathcal{T}) \times (\mathbb{R}^m)^{|V_D|} \to \mathbb{R}$ is the function defined in (2.6), and the set of feasible controls U_{ad} is given in (2.7). Observing that the operators $S_\omega^{(i)}\colon L^2(\mathcal{T}) \to L^2(\mathcal{T})$, $(i) \in E_D$, are linear and continuous while keeping the presence of the nonvanishing regularization term $\frac{\sigma}{2}\|u\|_{L^2(\mathcal{T})}^2$ in mind, the function $f(\cdot, \beta)$ is continuous and uniformly convex for each $\beta \in (\mathbb{R}^m)^{|V_D|}$. Furthermore, U_{ad} is, by construction, convex and closed. Thus, noting that $L^2(\mathcal{T})$ is a reflexive Banach space, (LL(β)) possesses a uniquely determined (global) minimizer, see e.g. Tröltzsch (2010, Theorem 2.16) for a similar result.

Proposition 2.5 *For each $\beta \in (\mathbb{R}^m)^{|V_D|}$, (LL($\beta$)) possesses a uniquely determined (global) minimizer.*

The above result motivates the following definition.

Definition 2.6 Let $\Psi\colon (\mathbb{R}^m)^{|V_D|} \to L^2(\mathcal{T})$ be the operator which assigns to each $\beta \in (\mathbb{R}^m)^{|V_D|}$ the uniquely determined (global) minimizer of (LL(β)).

In the subsequent result, we show via standard arguments that the mapping Ψ defined in Definition 2.6 is Lipschitz continuous.

Proposition 2.7 *The mapping Ψ is Lipschitz continuous.*

Proof For $\iota = 1, 2$, we choose $\beta_\iota \in (\mathbb{R}^m)^{|V_D|}$ and set $\bar{u}_\iota := \Psi(\beta_\iota)$. Convexity and continuous Fréchet differentiability of $f(\cdot, \beta_\iota)$ as well as convexity and closedness of U_{ad} yield that $\bar{u}_\iota$ is the global minimizer of (LL(β)) if and only if the condition

$$\forall u \in U_{\text{ad}}\colon \quad \big(f'(\bar{u}_\iota, \beta_\iota), u - \bar{u}_\iota\big)_{L^2(\mathcal{T})} \geq 0 \tag{2.9}$$

is valid, see (Tröltzsch 2010, Lemma 2.21). Above, $(\cdot,\cdot)_{L^2(\mathcal{T})} : L^2(\mathcal{T}) \times L^2(\mathcal{T}) \to \mathbb{R}$ denotes the standard inner product of the Hilbert space $L^2(\mathcal{T})$.

Applying the chain rule, we find an explicit formula for the derivative of $f(\cdot, \beta_\iota)$ with respect to u. More precisely, we have

$$f_u'(u, \beta_\iota) = \mathcal{A}(u) - \mathcal{B}(\beta_\iota) \tag{2.10}$$

for the continuous linear operators $\mathcal{A}\colon L^2(\mathcal{T}) \to L^2(\mathcal{T})$ and $\mathcal{B}\colon (\mathbb{R}^m)^{|V_D|} \to L^2(\mathcal{T})$ given by

$$\forall u \in L^2(\mathcal{T})\colon \quad \mathcal{A}(u) := \sum_{(i)\in E_D} ((S_\omega^{(i)})^* \circ S_\omega^{(i)})(u) + \sigma u,$$

where, for each $(i) \in E_D$, $(S_\omega^{(i)})^*\colon L^2(\mathcal{T}) \to L^2(\mathcal{T})$ is the adjoint of $S_\omega^{(i)}\colon L^2(\mathcal{T}) \to L^2(\mathcal{T})$, which is a linear, continuous operator again, see Remark 2.4, and

$$\forall \beta \in (\mathbb{R}^m)^{|V_D|}\colon \quad \mathcal{B}(\beta) := \sum_{(i)\in E_D} \sum_{\ell=1}^{m} \beta_\ell^{(i)} (S_\omega^{(i)})^* (D_\ell^{(i)}).$$

Hence, from (2.9) and (2.10), we find

$$\begin{aligned}(\mathcal{A}(\bar{u}_1) - \mathcal{B}(\beta_1), \bar{u}_2 - \bar{u}_1)_{L^2(\mathcal{T})} &\geq 0,\\ (\mathcal{A}(\bar{u}_2) - \mathcal{B}(\beta_2), \bar{u}_1 - \bar{u}_2)_{L^2(\mathcal{T})} &\geq 0.\end{aligned}$$

Adding up these inequalities and performing some rearrangements yields

$$(\mathcal{A}(\bar{u}_1 - \bar{u}_2), \bar{u}_1 - \bar{u}_2)_{L^2(\mathcal{T})} \leq (\mathcal{B}(\beta_1 - \beta_2), \bar{u}_1 - \bar{u}_2)_{L^2(\mathcal{T})}. \tag{2.11}$$

By definition of $\mathcal{A}$, we find

$$\begin{aligned}&(\mathcal{A}(\bar{u}_1 - \bar{u}_2), \bar{u}_1 - \bar{u}_2)_{L^2(\mathcal{T})}\\ &= \sum_{(i)\in E_D} \left(((S_\omega^{(i)})^* \circ S_\omega^{(i)})(\bar{u}_1 - \bar{u}_2), \bar{u}_1 - \bar{u}_2 \right)_{L^2(\mathcal{T})} + \sigma \|\bar{u}_1 - \bar{u}_2\|_{L^2(\mathcal{T})}^2\\ &= \sum_{(i)\in E_D} \|S_\omega^{(i)}(\bar{u}_1 - \bar{u}_2)\|_{L^2(\mathcal{T})}^2 + \sigma \|\bar{u}_1 - \bar{u}_2\|_{L^2(\mathcal{T})}^2\\ &\geq \sigma \|\bar{u}_1 - \bar{u}_2\|_{L^2(\mathcal{T})}^2,\end{aligned}$$

and due to the continuity of $\mathcal{B}$, there is a constant $\kappa > 0$, not depending on β_1 and β_2, such that

$$\begin{aligned}(\mathcal{B}(\beta_1 - \beta_2), \bar{u}_1 - \bar{u}_2)_{L^2(\mathcal{T})} &\leq \|\mathcal{B}(\beta_1 - \beta_2)\|_{L^2(\mathcal{T})} \|\bar{u}_1 - \bar{u}_2\|_{L^2(\mathcal{T})}\\ &\leq \kappa \|\beta_1 - \beta_2\|_{(\mathbb{R}^m)^{|V_D|}} \|\bar{u}_1 - \bar{u}_2\|_{L^2(\mathcal{T})}.\end{aligned}$$

Combining this with (2.11), we end up with

$$\|\bar{u}_1 - \bar{u}_2\|_{L^2(\mathcal{T})} \leq (\kappa/\sigma) \|\beta_1 - \beta_2\|_{(\mathbb{R}^m)^{|V_D|}},$$

which shows the desired Lipschitzness of Ψ. □

Let us close this subsection with some remarks.

Remark 2.8 (a) Let us mention that whenever the box constraints in the optimization problem (LL(β)) are dropped, i.e., $u_a \equiv -\infty$ and $u_b \equiv \infty$ in (2.7), then the associated solution operator Ψ is linear and continuous (as the operator $\mathcal{A}$, defined in the proof of Proposition 2.7, is coercive and, thus, as a consequence of the Lax–Milgram lemma, see e.g. Dobrowolski (2006, Theorem 2.29), continuously invertible).

(b) For the theory in this paper, it is essential that the dynamics in (LL(β)) are linear as this, together with the structure of the objective function, guarantees that, for fixed $\beta \in (\mathbb{R}^m)^{|V_D|}$, (LL($\beta$)) is a convex optimization problem which can be solved to (global) optimality without any difficulty. Recall that solving the lower-level problem globally is an intrinsic assumption in bilevel optimization. In case where (2.1) is replaced by a nonlinear hyperbolic conservation law, it first has to be studied whether (LL(β)) actually possesses a global solution, which can be done in line with the findings in Keimer (2014). The far more challenging task is to find a procedure which reliably computes the global minimizer of (LL(β)), which is a nontrivial problem in the presence of nonlinear dynamics as additional local minimizers and stationary points, which are not even local minimizers, may exist.

2.2 The upper-level problem

To motivate the reconstruction problem, we first consider the optimal control problem

$$\min_{z,u}\{g(z,u)\,|\,z = S(u),\ u \in U_{\mathrm{ad}}\} \tag{2.12}$$

where $g\colon C(\overline{\Omega}, L^2(\mathcal{T},\mathbb{R}^n)) \times L^2(\mathcal{T}) \to \mathbb{R}$ is a classical tracking-type function given by

$$g(z,u) := \frac{1}{2}\sum_{(i)\in E_D} \|z^{(i)}(\cdot,\omega) - D_{\mathrm{d}}^{(i)}\|^2_{L^2(\mathcal{T})} + \frac{\sigma}{2}\,\|u\|^2_{L^2(\mathcal{T})}$$

for each $z \in C(\overline{\Omega}, L^2(\mathcal{T},\mathbb{R}^n))$ and $u \in L^2(\mathcal{T})$, and U_{ad} is the set of feasible controls defined in (2.7). In (2.12), S denotes the solution operator associated with the hyperbolic conservation law (2.1), see Definition 2.3. Furthermore, $D_{\mathrm{d}}^{(i)} \in L^2(\mathcal{T})$, $(i) \in E_D$, is some desired demand at vertex v_i which shall be approximated by the associated components of the network flow resulting from a suitable choice of the control function u.

We assume that, e.g., by numerical experiments, $p \in \mathbb{N}$ (approximate) pairs of solutions $(z_{\mathrm{o},r}, u_{\mathrm{o},r}) \in C(\overline{\Omega}, L^2(\mathcal{T},\mathbb{R}^n)) \times L^2(\mathcal{T})$, $r = 1,\dots,p$, of (2.12) have been obtained for noisy desired demands, or that the measurement itself has been inexact so that $(z_{\mathrm{o},r}, u_{\mathrm{o},r})$ on their own are noisy. Let us emphasize that $z_{\mathrm{o},r}$ is some (noisy) state corresponding to $u_{\mathrm{o},r}$ for each $r = 1,\dots,p$, i.e., $z_{\mathrm{o},r} \approx S(u_{\mathrm{o},r})$. Our goal is to reconstruct the functions $D_{\mathrm{d}}^{(i)}$, $(i) \in E_D$, from these observations. In order to do so, we presume that, for suitably chosen $\beta^{(i)} \in \Lambda^m$, where Λ^m has been defined in (2.8), we can ensure

$$D_{\mathrm{d}}^{(i)} \approx \sum_{\ell=1}^{m} \beta_{\ell}^{(i)} D_{\ell}^{(i)}$$

for all $(i) \in E_D$, where $D_1^{(i)}, \ldots, D_m^{(i)}$ are the available prototypical demand profiles we already mentioned in Sect. 2.1.3. Hence, (LL(β)) can be interpreted as a special instance of (2.12).

In this regard, the reconstruction task can be modeled via the bilevel optimization problem

$$\min_{\beta,u} \left\{ \frac{1}{2} \sum_{r=1}^{p} \left(\left\| \mathcal{C}(S(u)) - \mathcal{C}(z_{\mathrm{o},r}) \right\|_{O_z}^2 + \left\| \mathcal{D}(u) - \mathcal{D}(u_{\mathrm{o},r}) \right\|_{O_u}^2 \right) \;\middle|\; \begin{array}{l} \beta \in (\Lambda^m)^{|V_D|} \\ u = \Psi(\beta) \end{array} \right\}. \tag{UL}$$

Here, some linear, continuous mapping $\mathcal{C}\colon C(\overline{\Omega}, L^2(\mathcal{T}, \mathbb{R}^n)) \to O_z$ plays the role of an observation operator that is applied to the network flows and the observed flows. Their difference is measured in some observation space O_z. Similarly, the linear, continuous mapping $\mathcal{D}\colon L^2(\mathcal{T}) \to O_u$ plays the role of an observation operator addressing the inflow, with O_u being yet another observation space. In order to obtain differentiability in function space of the objective function in (UL), it is desirable that O_z and O_u are Hilbert spaces, respectively, but this property is not required for the analysis in this paper. It should be noted that the model (UL) merely exploits the observations $(\mathcal{C}(z_{\mathrm{o},r}), \mathcal{D}(u_{\mathrm{o},r})) \in O_z \times O_u$ instead of the full approximate solutions $(z_{\mathrm{o},r}, u_{\mathrm{o},r}) \in C(\overline{\Omega}, L^2(\mathcal{T}, \mathbb{R}^n)) \times L^2(\mathcal{T})$, $r = 1, \ldots, p$, for the construction of the upper-level objective function. The latter fact allows for an efficient collection of data, depending on the precise structure of $\mathcal{C}$ and $\mathcal{D}$. In principle, it is also possible to use nonlinear, continuous observation operators in (UL), but for our purposes, linear, continuous operators are sufficient. Let us also recall that Ψ denotes the solution operator associated with the lower-level problem (LL(β)), see Definition 2.6. As already pointed out in Sect. 2.1.3, it might also be reasonable to remove the constraint $\beta \in (\Lambda^m)^{|V_D|}$ from (UL), resulting in a simpler problem.

We would like to mention a prototypical choice for the operator $\mathcal{C}$ here. It seems to be a reasonable idea to inspect the behavior of the flow along certain parts of (selected) edges pointing towards demand vertices from V_D. Thus, for some nonempty set $E' \subset E_D$ and (potentially trivial) closed intervals $I^{(i)} \subset \overline{\Omega}$, $(i) \in E'$, one could exploit $\mathcal{C}\colon C(\overline{\Omega}, L^2(\mathcal{T}, \mathbb{R}^n)) \to \prod_{(i)\in E'} C(I^{(i)}, L^2(\mathcal{T}))$ given by

$$\forall z \in C(\overline{\Omega}, L^2(\mathcal{T}, \mathbb{R}^n))\colon \quad \mathcal{C}(z) := \left(z^{(i)}(\cdot,\cdot)|_{\mathcal{T}\times I^{(i)}} \right)_{(i)\in E'}.$$

Particularly, one can choose $I^{(i)} := \{\omega\}$ for each $(i) \in E'$ in order to compare network flows and observed flows merely by means of the outflow at certain demand vertices. Note that the operator $\mathcal{C}$ might be also restricted in time, see Sect. 3.1 and our numerical experiments in Sect. 3.3.4. The operator $\mathcal{D}$ may be chosen similarly, restricting the observation of the inflow in time, including the trivial case where $\mathcal{D}$ is the identity. Whenever $\mathcal{D}$ is chosen to be the zero operator, the inflow is not observed.

Let us demonstrate that the reconstruction problem (UL) possesses an optimal solution.

Proposition 2.9 *The optimization problem (UL) possesses a globally optimal solution.*

Proof We note that (UL) can be transferred into a finite-dimensional optimization problem by plugging the lower-level solution operator Ψ into the objective function. It is obvious that a point $\beta \in (\mathbb{R}^m)^{|V_D|}$ is a global minimizer of the resulting control-reduced problem if and only if $(\beta, \Psi(\beta))$ is a global minimizer of (UL). By continuity of Ψ, see Proposition 2.7, and continuity of $\mathcal{C}$ as well as $\mathcal{D}$, the objective function of the reduced problem is then continuous, while its feasible set $(\Lambda^m)^{|V_D|}$ is nonempty and compact. Thus, the reduced problem possesses a global minimizer $\bar{\beta} \in (\mathbb{R}^m)^{|V_D|}$ by the Weierstraß theorem, and this yields that $(\bar{\beta}, \Psi(\bar{\beta}))$ solves (UL) to global optimality. □

Although being globally Lipschitz continuous, see Proposition 2.7, the lower-level solution operator Ψ, which, at least in discretized form, see Appendix A, can be represented as the composition of a linear, continuous operator and the projection onto U_{ad}, is likely to be nonsmooth apart from the special situation where no control constraints are present, see Remark 2.8. Eliminating the control variable u in (UL) by plugging Ψ into the objective function, thus, leads to a finite-dimensional but nonconvex, nonsmooth optimization problem with polyhedral constraints. Whenever $U_{\mathrm{ad}} = L^2(\mathcal{T})$ holds, Ψ is linear, see Remark 2.8 again, and (UL) is actually a convex optimization problem. In this particular situation, numerical methods which identify stationary points of (UL) may already compute global minimizers of the problem. This is a rare property in hierarchical optimization where the multilevel structure is, typically, a source of nonconvexity and nonsmoothness, and this problem we also face in the general setting where control constraints are present.

3 Numerical solution and computational results

In this section, we first describe how (UL) can be solved in numerical practice. Second, results of some computational experiments are presented.

3.1 Numerical solution of the problem

For the network discretization, we choose a time grid $(t_j)_{j=1}^J$ of $J \in \mathbb{N}$ discretization points such that $t_j := (j-1)\Delta t$ for all $j \in \{1, \dots, J\}$, where $\Delta t > 0$ is a given temporal stepsize, and a spatial discretization of each edge (i), represented by the interval $(0, \omega)$, as $(x_q^{(i)})_{q=1}^{L^{(i)}}$, where $L^{(i)} \in \mathbb{N}$ is the number of discretization points, $x_q^{(i)} := (q-1)\Delta x^{(i)}$ for all $q \in \{1, \dots, L^{(i)}\}$, and $\Delta x^{(i)} > 0$ is the spatial stepsize for edge (i). The transported quantities $z_{j,q}^{(i)}$ at time t_j and position $x_q^{(i)}$ given by the PDE in (2.1a) are calculated using a left-sided upwind scheme, i.e.,

$$z_{j,q}^{(i)} = z_{j-1,q}^{(i)} - \frac{\Delta t}{\Delta x^{(i)}} \lambda^{(i)} \left(z_{j-1,q}^{(i)} - z_{j-1,q-1}^{(i)} \right), \quad j \in \{2, \dots, J\},\ q \in \{2, \dots, L^{(i)}\}.$$

We also note that (2.1b) translates into $z^{(i)}_{1,q} = 0$ for all $q \in \{1, \dots, L^{(i)}\}$. At the junctions, according to (2.1c) and (2.1d), we require

$$z^{(1)}_{j,1} = \frac{u_j}{\lambda^{(1)}}, \qquad z^{(k)}_{j,1} = \alpha_{i,k} \frac{\lambda^{(i)}}{\lambda^{(k)}} z^{(i)}_{j,L^{(i)}}, \quad v_i \in V_I,\ (k) \in E^+(i),\ j \in \{1, \dots, J\}$$

where $u_j := u(t_j)$ for all $j \in \{1, \dots, J\}$. For $\frac{\Delta t}{\Delta x^{(i)}} \lambda^{(i)} = 1$, the upwind scheme shows no diffusion. Therefore, we set $\Delta x^{(i)} := \lambda^{(i)} \Delta t$ which leads to different spatial grids on the different edges whenever the respective coefficients $\lambda^{(i)}$ are not the same.

We use this discretization for a finite differences approximation of the lower-level problem (LL(β)). We define $S^{(i),L^{(i)}} \in \mathbb{R}^{J \times J}$ to be the (discrete) realization of $S^{(i)}_\omega$ such that $\sum_{\nu=1}^{J} S^{(i),L^{(i)}}_{j,\nu} u_\nu$ approximates the influence of the discretized inflow on the density $z^{(i)}_{j,L^{(i)}}$ at time t_j and spatial point ω. Further, we denote the discrete versions of the demand profiles $D^{(i)}_1, \dots, D^{(i)}_m$ for edge $(i) \in E_D$ by $\tilde{D}^{(i)}_1, \dots, \tilde{D}^{(i)}_m \in \mathbb{R}^J$.

For our computations, we will exploit that the columns of $S^{(i),L^{(i)}}$ are orthogonal to each other. This is the case since, due to the special structure of the PDEs, there is a one-to-one correspondence between the inflow into the system and the outflow out of the system. Therefore, in the discretized setting, there is a unique time point for the inflow that determines the outflow at the corresponding outflow time. This property enforces the matrix $S^{(i),L^{(i)}}$ to be nonzero on its subdiagonal. Consequently, $S^{(i),L^{(i)}}$ is orthogonal.

For a given convex combination of base demands by the vector β and using (2.10), we obtain the optimal inflow in the discretized setting in the absence of control constraints when solving the linear system $Au - B\beta = 0$ where A is given by

$$A := \sum_{(i) \in E_D} \left(S^{(i),L^{(i)}}\right)^\top \left(S^{(i),L^{(i)}}\right) + \sigma \mathbb{I}_J,$$

where $\mathbb{I}_J \in \mathbb{R}^{J \times J}$ is the identity matrix, and

$$B := \left[Q^{(i)}\right]_{(i) \in E_D}.$$

Above, for each $(i) \in E_D$, $Q^{(i)} \in \mathbb{R}^{J \times m}$ is given by

$$Q^{(i)} := \left[\left(S^{(i),L^{(i)}}\right)^\top \tilde{D}^{(i)}_1 \ \dots \ \left(S^{(i),L^{(i)}}\right)^\top \tilde{D}^{(i)}_m\right].$$

We note that the discretized lower-level problem is equivalent to

$$\min_u \{\tfrac{1}{2} u^\top A u - (B\beta)^\top u \mid u_\mathrm{a} \le u \le u_\mathrm{b}\},$$

where $u_{\mathrm{a},j} := u_\mathrm{a}(t_j)$ and $u_{\mathrm{b},j} := u_\mathrm{b}(t_j)$ for all $j = 1, \dots, J$. We obtain the solution of this problem by projecting the solution of the linear equation $Au - B\beta = 0$ onto

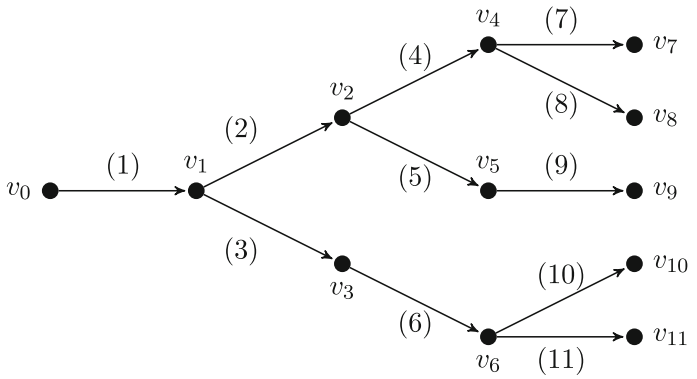

Fig. 2 The network considered in Sect. 3.3 with $V_D = \{v_7, v_8, v_9, v_{10}, v_{11}\}$, $V_I = \{v_1, v_2, v_3, v_4, v_5, v_6\}$, and $E_D = \{(7), (8), (9), (10), (11)\}$

the feasible box, since A is a diagonal positive definite matrix by orthogonality of $S^{(i),L^{(i)}}$, $(i) \in E_D$, see Appendix A for details.

For the upper-level problem (UL), we apply the same discretization technique with different stepsizes, see Sect. 3.3, and consider, if not specified differently, the observation operator $\mathcal{C}$ in which we only observe the densities at the demand vertices from V_D, corresponding to the last discretization points of the edges in E_D, as well as at the first discretization point of edge (1), monitoring the inflow at v_0. Additionally, $\mathcal{D}$ is the zero operator in our experiments. Further details and some numerical examples are explained in Sect. 3.3 where it is also described how $\mathcal{C}$ and $\mathcal{D}$ can be adjusted.

Inserting the discretized solution operator of the lower-level problem into the objective function of the discretized upper-level problem results in a nonsmooth optimization problem with affine constraints, and we solve the latter using MATLAB's `patternsearch` solver in default mode. We want to emphasize that the performance of this optimization routine heavily depends on the initial point that is handed over to the solver. This, however, is not surprising as the considered nonsmooth problem of interest is nonconvex and, thus, likely to possess several local minimizers and stationary points which are different from its global minimizers. As the model is designed to reconstruct certain reference parameters from noisy data, we initialize `patternsearch` with a perturbed version of these reference parameters to face this problem. We note that, in the absence of lower-level control constraints, the resulting single-level problem is a simple convex quadratic problem which can be solved, exemplary, with the aid of MATLAB's `quadprog` routine, and the aforementioned issues do not occur.

3.2 General set-up of experiments

We consider the tree-shaped network presented in Fig. 2 in which each edge has a length of $\omega = 1$.

The velocities are chosen identically for all edges, we use $\lambda^{(i)} = 10, i = 1, \ldots, 11$. The stepsizes are given by $\Delta t = \frac{1}{60}$, $\Delta x = \frac{1}{6}$ for the backward calculation and

$\Delta t = \frac{1}{70}$, $\Delta x = \frac{1}{7}$ for the forward calculation, which are chosen differently to avoid an inverse crime, see (Colton and Kress 2013, page 154), for the unconstrained examples, and $\Delta t = \frac{1}{20}$, $\Delta x = \frac{1}{2}$ (backward calculation), $\Delta t = \frac{1}{30}$, $\Delta x = \frac{1}{3}$ (forward calculation) when applying constraints to the inflow in order keep reasonable running times. Note that $\Delta x^{(i)} = \Delta x$ is exploited, $i = 1, \dots, 11$. In both cases, the Courant–Friedrichs–Lewy condition holds true with equality, i.e., $\frac{\Delta t}{\Delta x}\lambda^{(i)} = 1$, $i = 1, \dots, 11$, to avoid diffusion in the numerical scheme. The distribution parameters are set to

$$\begin{aligned} &\alpha_{1,2} = 0.65, \quad &&\alpha_{2,4} = 0.7, \quad &&\alpha_{4,7} = 0.5, \quad &&\alpha_{6,10} = 0.4, \\ &\alpha_{1,3} = 0.35, \quad &&\alpha_{2,5} = 0.3, \quad &&\alpha_{4,8} = 0.5, \quad &&\alpha_{6,11} = 0.6. \end{aligned}$$

We consider the evolution of the demand within one week, i.e., $T = 168$ where one time unit represents one hour and assume four underlying base demand levels which are visualized in Fig. 3 and chosen as

- a time constant level of the demand: $D_1(t) = 4$,
- a daily varying level at which we attain the highest level in the morning: $D_2(t) = 2 + \sin(\pi(t-2)/12)$,
- a daily varying level at which we attain the highest level in the afternoon: $D_3(t) = 2 + \sin(\pi(t-10)/12)$,
- a level that illustrates the lower demand during the weekend: $D_4(t) = \mathbb{1}_{[0,120]}(t)$.

These choices can similarly be found for example for the electricity market in Coskun and Korn (2021) and describe the identified two-peak pattern of demand in the intraday market (D_2, D_3) as well as the phenomenon referred to as the *weekend effect* (D_4). For the prototypical demand profiles, we make use of $D_\ell^{(i)} := \hat{d}^{(i)} D_\ell$, $i \in \{7, \dots, 11\}$, $\ell \in \{1, 2, 3, 4\}$, where

$$\hat{d}^{(7)} = 0.2275, \quad \hat{d}^{(8)} = 0.2275, \quad \hat{d}^{(9)} = 0.195, \quad \hat{d}^{(10)} = 0.14, \quad \hat{d}^{(11)} = 0.21.$$

This choice proportionally accounts for the different distribution parameters in the network. The historical observations are basically generated using the initial weights

$$(\beta_1, \beta_2, \beta_3, \beta_4) = (0.2, 0.15, 0.2, 0.45). \tag{3.1}$$

In every time step and for every demand vertex, the base demand levels are perturbed by random variables

$$Z_1^{(i)} \sim \mathcal{N}(0, 1), \quad Z_2^{(i)} \sim \mathcal{N}(0, 1/4), \quad Z_3^{(i)} \sim \mathcal{N}(0, 1/4), \quad Z_4^{(i)} \sim \mathcal{N}(0, 1/4),$$

such that the historically desired demands are given by realizations of

$$D_{\mathrm{d}}^{(i)} = \sum_{\ell=1}^{4} \beta_\ell \hat{d}^{(i)} \left(D_\ell + Z_\ell^{(i)} \right), \quad i \in \{7, \dots, 11\}. \tag{3.2}$$

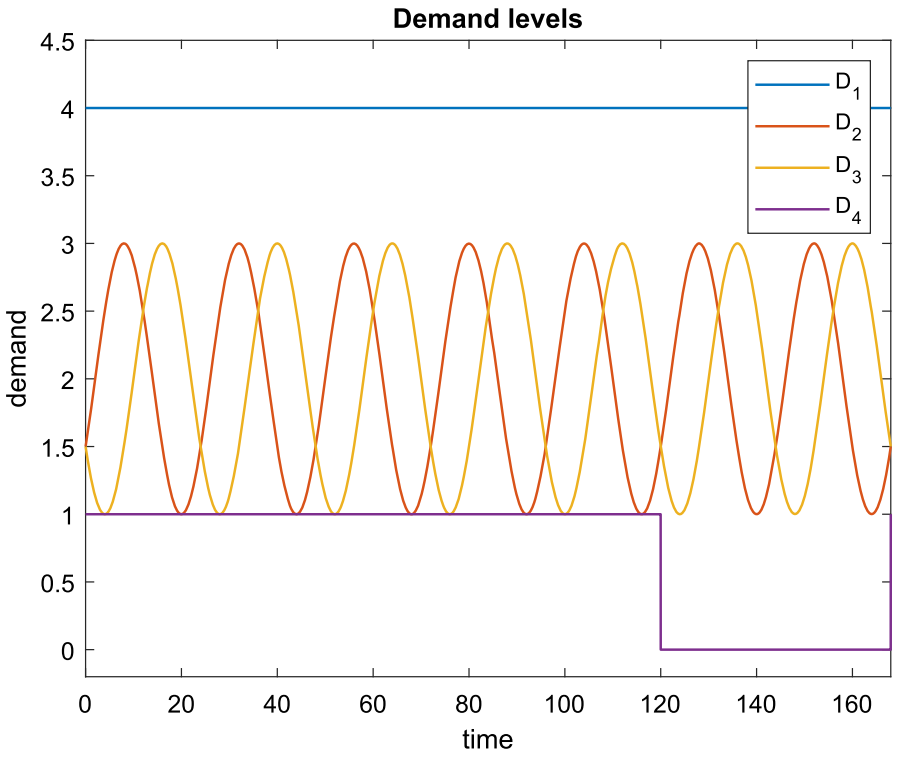

Fig. 3 Illustration of the four base demand levels

The historically observed pairs (z_o, u_o) are computed as solutions of the associated problem (2.12).

3.3 Documentation of experiments

In the following, we investigate different variants of the bilevel optimization problem (UL). The standard version is presented in Sect. 3.3.1, and settings with additional perturbations in the historical observations are shown in Sects. 3.3.2 and 3.3.3. A time-restricted observation operator $\mathcal{C}$ is investigated in Sect. 3.3.4. All subsections are constructed in a similar way. First, we present exemplary historical demand observations, then we provide a comparison of the in- and outflows for the means of the historical observations and the initially chosen β as well as for the reconstructed β in a framework without an inflow constraint, which can also be considered as a framework with a high constraint that does not really affect the inflow. These illustrations are presented for the inflow vertex and the demand vertex v_7 (the behavior at all other demand vertices is similar). We can verify that, on the one hand, the optimal inflows are calculated correctly and, on the other hand, see whether the reconstruction of the weights β was successful. The second aspect is further underlined by a table presenting the means and variances for β of a Monte Carlo simulation of $N = 40$ runs for

different numbers of historical observations p. Second, we repeat the investigations of each subcase based on a medium inflow constraint $u_b \equiv 2$ and a low inflow constraint $u_b \equiv 1.5$, where we also ensure nonnegative inflows, i.e., $u_a \equiv 0$, the latter being nonrestrictive as the desired demand at the vertices in V_D is nonnegative.

3.3.1 Standard model without additional adjustments

In this scenario, no further perturbations or model changes are included, and we consider the framework presented in the previous sections. Three examples for historical observations are given in Fig. 4 which show the sinusoidal behavior of demand, as well as the drop for $t > 120$ during the weekend. Furthermore, we detect the stochastic noise in the demands, however, still verify that the demands show a very similar structure. The comparison of the inflow and outflow for demand vertex v_7 are presented in Fig. 5, where the blue curve shows the mean values of the $p = 6$ historical observations, the yellow dotted line represents the curve for the *true* β given in (3.1), and the red line the in- or outflow for the reconstructed β. All considerations were made without constraining the inflow control. It can be concluded that all three curves match very well, which means that, on the one hand, the inflow is calculated appropriately and, on the other hand, also the weights of the base demands are reobtained very well. The outflow behavior at the demand vertices $v_8, \ldots, v_{11}$ shows similar patterns and is (for brevity of presentation) not illustrated. At the beginning and the end of the considered time horizon, some curves in Fig. 5 decay to zero or show a jump. This can be explained by the fact that around time $t = 0$, it takes some time until (starting from an empty system) the first inserted quantity reaches the demand vertex. Therefore, the outflows are zero in the very beginning of the time period. Conversely, the inflow for times close to $T = 168$ vanishes, since these quantities do not reach the demand nodes within the considered time horizon. The increase at $T = 168$ in the outflow figure can be explained by considering $T = 168$ to be Monday already, where the demand is larger again. Similar artifacts show up in some other figures in this section due to analogous reasons.

Table 1 shows the means and variances of the reconstructed weights for the base demands for different numbers of perturbed historical observations in a Monte Carlo simulation of $N = 40$ runs and underlines the results from Fig. 5 quantitatively. As it can be expected for larger numbers of historical observations, the means approach the values in (3.1) and the variances in the runs decrease in the number of historical observations p.

Accounting for a potential constraint on the inflow, we compare a scenario where the inflow is limited to 2 (medium constraint) and 1.5 (low constraint). We repeat the idea of Fig. 5 in Fig. 6 emphasizing that, except for the constraint, all other quantities remain unchanged. However, the demand illustration seems to be less fluctuating which can be explained by the coarser discretization grid that is used for the constrained optimization. In the medium constraint case, we observe that the in- and outflow follow the unconstrained case but are truncated at the very highest peaks and otherwise follow the averaged demand well. Regarding the reconstruction of the weights of the base demand levels when zooming in, one can still observe a quite good match in the in- and outflows of the optimized and initial choices of β. Table 2 underlines this observation,

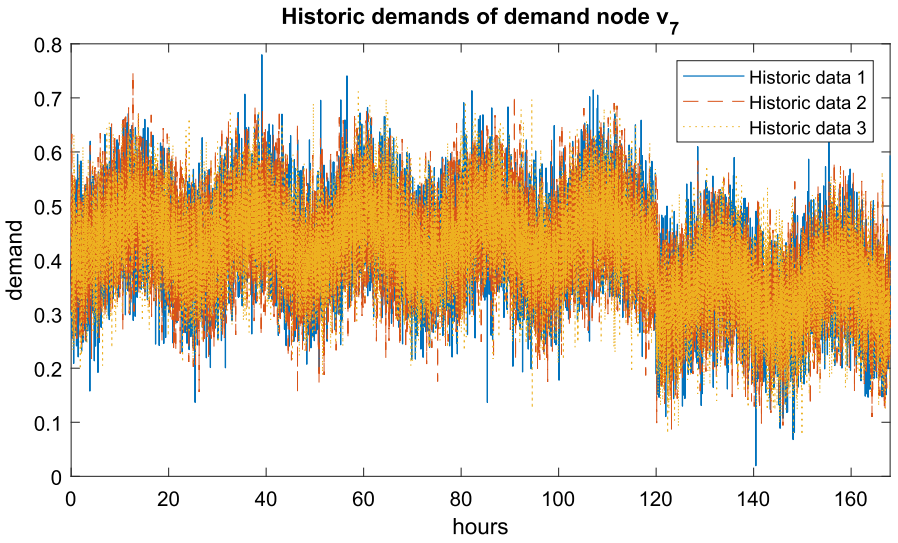

Fig. 4 Three of the perturbed historically observed demands for demand vertex v_7 in the case of Sect. 3.3.1

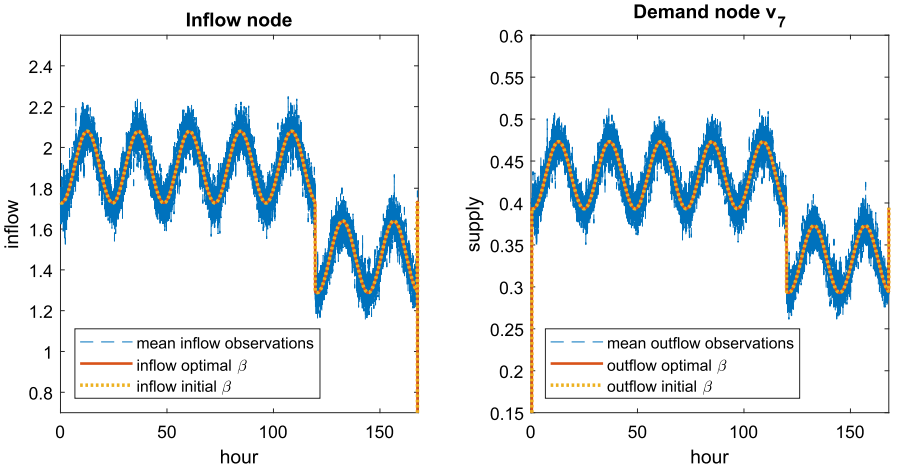

Fig. 5 A comparison between the mean realization of the $p = 6$ historical in- and outflows with the in- and outflow for the reconstructed β in the case of Sect. 3.3.1 and the initial β

Table 1 Means and variances of the reobtained weights for the base demands for different choices of the number of perturbed historical observations p in the setting of Sect. 3.3.1

	mean				variance			
	$p = 1$	$p = 6$	$p = 20$	$p = 200$	$p = 1$	$p = 6$	$p = 20$	$p = 200$
β_1	0.2003	0.2000	0.1999	0.2000	2.16e−06	0.25e−06	0.16e−06	0.10e−07
β_2	0.1496	0.1499	0.1500	0.1500	6.65e−06	0.42e−06	0.29e−06	0.21e−07
β_3	0.2001	0.2001	0.2002	0.2000	2.82e−06	0.87e−06	0.31e−06	0.18e−07
β_4	0.4503	0.4500	0.4499	0.4500	4.16e−06	0.57e−06	0.34e−06	0.21e−07

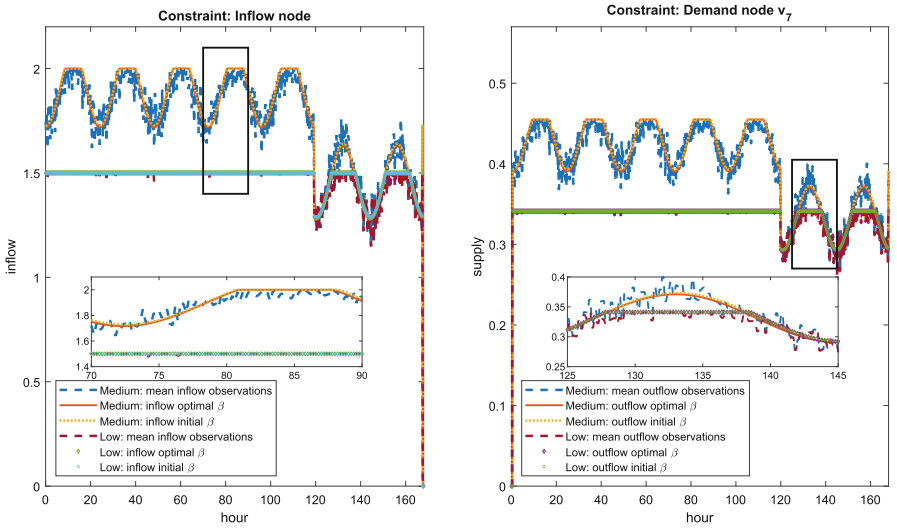

Fig. 6 A comparison between the mean realization of the $p = 6$ historical in- and outflows with the in- and outflow for the reconstructed β in the case of Sect. 3.3.1 and the initial β with two different inflow constraints

Table 2 Means and variances of the reobtained weights for the base demands for different choices of the number of perturbed historical observations p in the setting of Sect. 3.3.1 with additional inflow constraints

	mean				variance			
	medium		low		medium		low	
	$p = 6$	$p = 200$	$p = 6$	$p = 200$	$p = 6$	$p = 200$	$p = 6$	$p = 200$
β_1	0.1960	0.1972	0.2460	0.2474	2.87e−06	0.11e−06	0.83e−04	0.11e−05
β_2	0.1549	0.1536	0.0997	0.0988	5.93e−06	0.22e−06	0.91e−04	0.10e−05
β_3	0.1997	0.1997	0.1297	0.1284	6.77e−06	0.35e−06	1.10e−04	0.21e−05
β_4	0.4493	0.4495	0.5245	0.5254	6.24e−06	0.30e−06	1.11e−04	0.15e−05

but shows a small deviation especially in the parameters β_1 and β_2 compared to the unrestricted case. For the low constraint, the inflow is cut from Monday to Friday and in some peak times also during the weekend, so that most of the time demand cannot be satisfied on average. Then the reconstruction task is also not successful, and we can observe a visible mismatch in the green circles (associated to the optimal outflow for the initial β) and purple diamonds (representing the outflow for the reconstructed β) during the weekend. Referring again to Table 2, one can see that there is a large deviation in the reconstructed values of β, where the very low values of β_2 and β_3 are particularly striking. This effect can be explained by the fact that D_2 and D_3 are the sinusoidal components of demand and that the observations are smoothed and truncated at the majority of time.

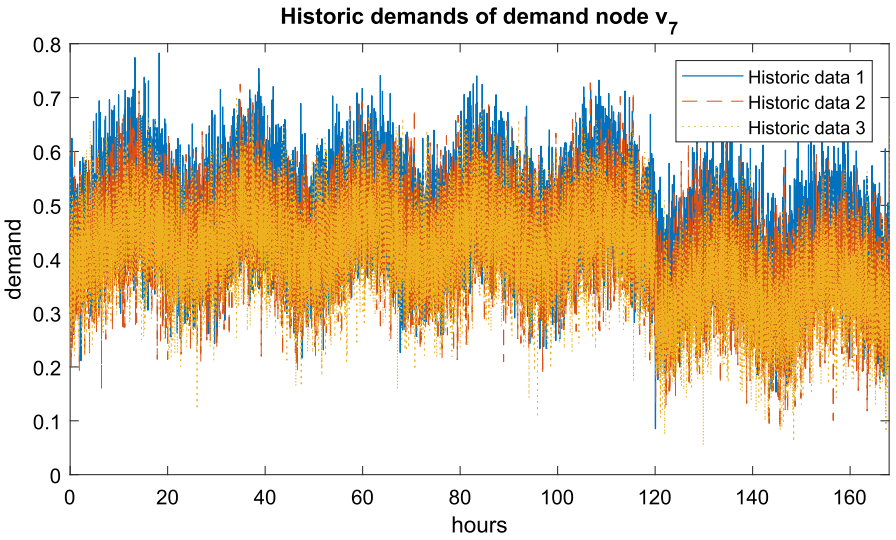

Fig. 7 Three of the perturbed historically observed demands for demand vertex v_7 in the case of Sect. 3.3.2

3.3.2 Results with additional noise in the weights β

In addition to the investigation of Sect. 3.3.1, we introduce a structural and uncertain deviation in the choice of β, when generating the historically desired demand in (3.2). We assume that the uncertainty mainly comes into play for β_4 such that for any historical observation, the weights for the demand levels are chosen as

$$(\beta_1, \beta_2, \beta_3, \beta_4) = \left(\frac{0.2}{1+\tilde{Z}}, \frac{0.15}{1+\tilde{Z}}, \frac{0.2}{1+\tilde{Z}}, \frac{0.45+\tilde{Z}}{1+\tilde{Z}} \right) \tag{3.3}$$

for a uniformly distributed random variable $\tilde{Z} \sim \mathcal{U}([-0.05, 0.05])$.

The results for some historical observations are presented below in Fig. 7. There is not only noise in the demands but also structurally different behavior due to different realizations of $\tilde{Z}$ in the weights of the demands. Therefore, the yellow curve of historic data 3 seems to be lower (corresponding to a larger value of $\tilde{Z}$) than the blue curve (corresponding to a smaller value of $\tilde{Z}$). Figure 8 shows the different in- and outflows which are supplemented by Table 3 showing the means and the variances of a Monte Carlo simulation for the reconstructed weights of the base demands for different numbers of perturbed historical observations. We observe that in Fig. 8, the expected outflow and inflow match quite well, but considering Table 3, it can be seen that the reconstruction is more difficult than in the standard setting. For small p, the reconstructed β deviates more significantly from the initial choice. For a larger number of observations p, the data indicates that the performances are improved and lead to good reconstructed values of β.

Also in this scenario, we investigate a constraint on the inflow control on a medium level of 2 and a low constraint of 1.5. Similar to Sect. 3.3.1, the reconstruction works at

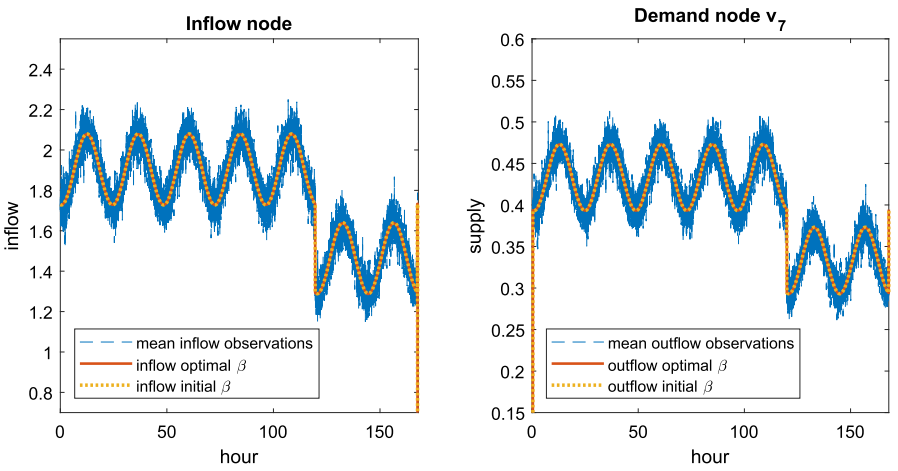

Fig. 8 A comparison between the mean realization of the $p = 6$ historical in- and outflows with the in- and outflow for the reconstructed β in the case of Sect. 3.3.2 and the initial β

Table 3 Means and variances of the reobtained weights for the base demands for different choices of the number of perturbed historical observations p in the setting of Sect. 3.3.2

	mean				variance			
	$p = 1$	$p = 6$	$p = 20$	$p = 200$	$p = 1$	$p = 6$	$p = 20$	$p = 200$
β_1	0.2012	0.2010	0.2001	0.2001	0.36e−04	0.08e−04	0.19e−05	0.01e−05
β_2	0.1497	0.1509	0.1500	0.1501	0.26e−04	0.04e−04	0.14e−05	0.01e−05
β_3	0.2013	0.2013	0.2003	0.2001	0.40e−04	0.06e−04	0.19e−05	0.01e−05
β_4	0.4477	0.4468	0.4496	0.4497	2.76e−04	0.49e−04	1.37e−05	0.08e−05

least satisfactorily in the medium constraint case, whereas it fails in the low constraint case. Nevertheless, in both cases, the average outflow matches the optimal outflow for the reconstructed β, see Fig. 9. Table 4 shows for $p \in \{6, 200\}$ the mean and the variance as the adapted version of Table 3 with medium and low inflow constraint, where the variances are similar but slightly higher than in the unconstrained framework. The observed effects are comparable to those obtained for the constrained but unperturbed regime in Table 2.

3.3.3 Results with changed base demand level D_4

This section is based on the investigations in Sect. 3.3.1. Instead of perturbing β, we assume that there is a structural deviation in the base demand levels. Particularly, we assume that in the generation of the observations, we adjust the base demand D_4 to $D_4(t) = \frac{3}{2}\mathbb{1}_{[0,120]}(t)$, which means that there is larger share of demand on weekdays. Furthermore, we omit the normalization restriction to the weights, i.e., we merely assume $\beta_\ell \geq 0$, $\ell \in \{1, \ldots, 4\}$, and drop the constraint $\sum_{\ell=1}^{4} \beta_\ell = 1$, since the increase in the base demand level should now be captured by a larger weight on

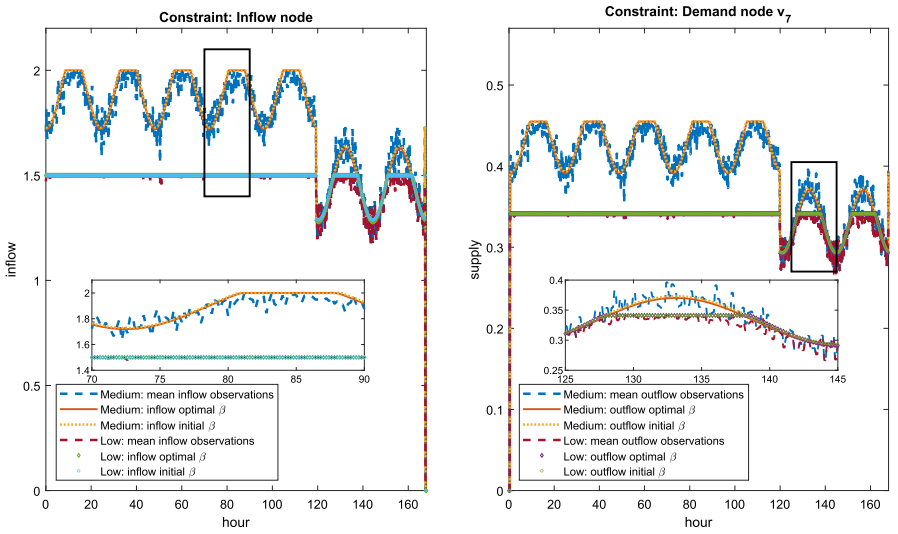

Fig. 9 A comparison between the mean realization of the $p = 6$ historical in- and outflows with the in- and outflow for the reconstructed β in the case of Sect. 3.3.2 and the initial β with two different inflow constraints

Table 4 Means and variances of the reobtained weights for the base demands for different choices of the number of perturbed historical observations p in the setting of Sect. 3.3.2 with additional inflow constraints

	mean				variance			
	medium		low		medium		low	
	$p = 6$	$p = 200$	$p = 6$	$p = 200$	$p = 6$	$p = 200$	$p = 6$	$p = 200$
β_1	0.1958	0.1965	0.2494	0.2518	0.06e−04	0.02e−05	1.01e−04	0.18e−05
β_2	0.1548	0.1539	0.0923	0.0909	0.10e−04	0.06e−05	0.85e−04	0.10e−05
β_3	0.1996	0.1997	0.1285	0.1262	0.10e−04	0.09e−05	1.21e−04	0.28e−05
β_4	0.4498	0.4499	0.5297	0.5310	0.36e−04	0.27e−05	1.09e−04	0.24e−05

β_4. Note that we still use $D_4(t) = \mathbb{1}_{[0,120]}(t)$ in the lower-level objective function from (2.6) for the reconstruction task. Similar to Sect. 3.3.1, examples of the historical observations are presented in Fig. 10 which now show a larger difference between the weekday demand and the weekend demand induced by the larger value in D_4. Again, Fig. 11 shows the in- and outflows for the means of the observations (blue), the initial β from (3.1) (yellow dotted), and the reconstructed β (red). One can see that the in- and outflow of the initial β do not match from Monday to Friday, but do on the weekend, since they are not able to take into account the change in D_4. The reconstructed weights yield the correct inflows and outflows with respect to the observations and manage to compensate the structural deviation in D_4. In Table 5, we observe that the values for β_1, β_2, and β_3 are very well reobtained with similar variances as in Table 1. The value of β_4 now exceeds significantly the initial value of 0.45. Recalling that the base demand level D_4 was increased from 1 to 1.5 at the lower-level stage, one notices that

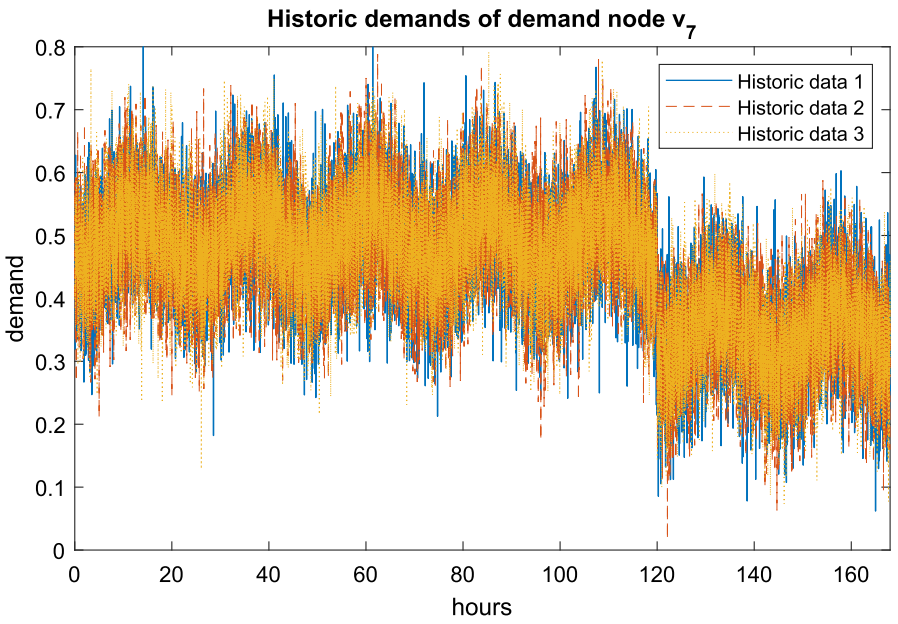

Fig. 10 Three of the perturbed historically observed demands for demand vertex v_7 in the case of Sect. 3.3.3

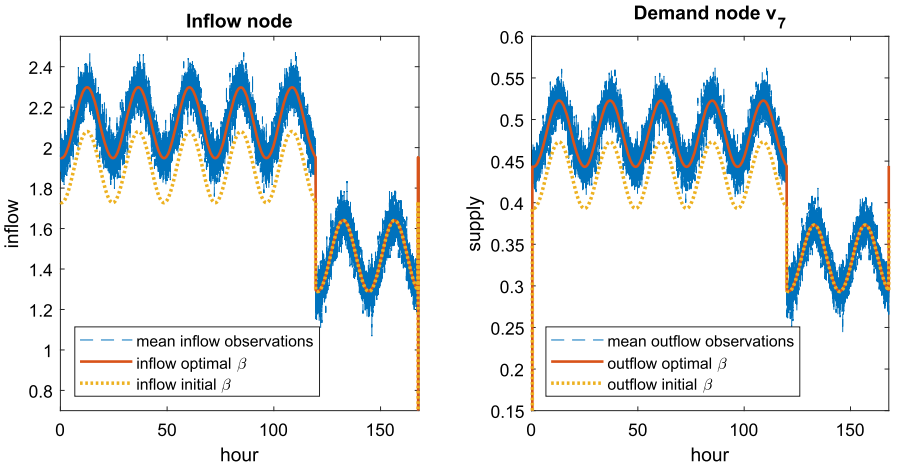

Fig. 11 A comparison between the mean realization of the $p = 6$ historical in- and outflows with the in- and outflow for the reconstructed β in the case of Sect. 3.3.3 and the initial β including the structural deviation in D_4

also the reconstructed value of β_4 increased by factor 1.5 to compensate to unchanged level of D_4 in the parameter reconstruction. This allows for a good reconstruction of the observation means, but as expected violates the normalization of the base demand weights.

Table 5 Means and variances of the reobtained weights for the base demands for different choices of the number of perturbed historical observations p with additive deviation in D_4 in the setting of Sect. 3.3.3

	mean				variance			
	$p = 1$	$p = 6$	$p = 20$	$p = 200$	$p = 1$	$p = 6$	$p = 20$	$p = 200$
β_1	0.1999	0.1998	0.1998	0.2000	0.59e−05	0.14e−05	0.03e−05	0.03e−06
β_2	0.1505	0.1499	0.1502	0.1499	0.77e−05	0.16e−05	0.03e−05	0.03e−06
β_3	0.2003	0.2002	0.2003	0.2000	0.53e−05	0.13e−05	0.03e−05	0.03e−06
β_4	0.6734	0.6752	0.6750	0.6749	1.20e−05	0.20e−05	0.04e−05	0.06e−06

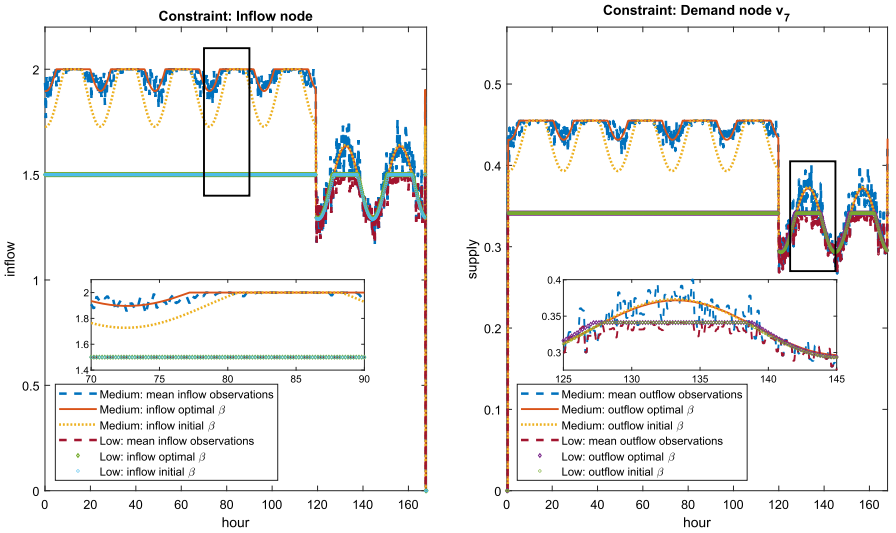

Fig. 12 A comparison between the mean realization of the $p = 6$ historical in- and outflows with the in- and outflow for the reconstructed β in the case of Sect. 3.3.3 and the initial β including the structural deviation in D_4 with two different inflow constraints

When adapting the base demand level accounting for the weekend effect with a medium constraint $u_b \equiv 2$, similar to the unconstrained case, we observe in Fig. 12 that the in- and outflow rates for the reconstructed β exceed those for the initial β, but are cut at the maximum inflow level of 2. Therefore, in Table 6, the values of the reconstructed β are very similar to the ones obtained in Table 5 without constraint, but have a lower value for β_4 due to the inflow constraint and the resulting lower observed supply. For the more restricted inflow control with $u_b \equiv 1.5$, the reconstructed β is far from the initial one, since by cutting off the inflow, we lose information about the true demand.

3.3.4 Results with no noise in β and observations only on Sunday

In this section, we consider another variant of the framework in Sect. 3.3.1 and do not introduce additional noise or deviations. Instead, we restrict the observation time of the historical data by adjusting the observation operators $\mathcal{C}$ and $\mathcal{D}$. Therefore, the

Table 6 Means and variances of the reobtained weights for the base demands for different choices of the number of perturbed historical observations p with additive deviation in D_4 in the setting of Sect. 3.3.3 with additional inflow constraints

	mean				variance			
	medium		low		medium		low	
	$p = 6$	$p = 200$	$p = 6$	$p = 200$	$p = 6$	$p = 200$	$p = 6$	$p = 200$
β_1	0.2056	0.2049	0.2429	0.2445	0.18e−04	0.07e−05	0.84e−04	0.14e−05
β_2	0.1474	0.1489	0.0993	0.0980	0.27e−04	0.08e−05	0.93e−04	0.12e−05
β_3	0.1915	0.1918	0.1379	0.1358	0.28e−04	0.10e−05	1.15e−04	0.26e−05
β_4	0.6111	0.6130	0.9867	0.9991	0.38e−04	0.08e−05	3.85e−04	8.18e−05

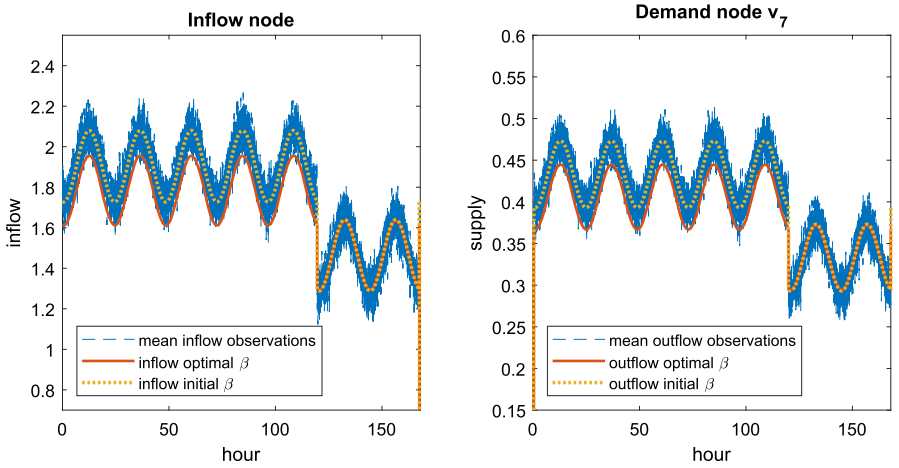

Fig. 13 A comparison between the mean realization of the $p = 6$ historical in- and outflows with the in- and outflow for the reconstructed β in the case of Sect. 3.3.4 and the initial β where observations can only be made on Sundays ($t \in [144, 168]$)

observation operators only consider $t \in [144, 168]$, i.e., historical data is only taken into account on Sundays, and the model is used to reestimate the choices of β from that knowledge for the entire week. Furthermore, to avoid hidden information on β_4 via the normalization constraint, similar to Sect. 3.3.3, we drop the condition $\sum_{\ell=1}^{4} \beta_\ell = 1$ in the optimization problem (UL) and merely require $\beta_\ell \geq 0$, $\ell \in \{1, \ldots, 4\}$. For the illustration of historical data, we refer to Fig. 4 in Sect. 3.3.1 as there are no differences in the historical data. In Fig. 13, for the in- and outflows, we observe an undersupply in the curve of the optimal β (red) from Monday to Friday. For the weekend, the reconstruction works fine, since past information is available for this time period. Table 7 underlines that there is no information on the choice of β_4. While the means seem to be close together in the Monte Carlo simulation for the different numbers of observations, the very large variances reveal that β_4 is arbitrary to choose in the case of restricted information. This, however, is not surprising as, on the one hand, the normalization condition on the weights has been dropped and, on the other hand, D_4 vanishes during the weekend.

Table 7 Means and variances of the reobtained weights for the base demands for different choices of the number of perturbed historical observations p with observations only for $t \in [144, 168]$ from Sect. 3.3.4

	mean				variance			
	$p = 1$	$p = 6$	$p = 20$	$p = 200$	$p = 1$	$p = 6$	$p = 20$	$p = 200$
β_1	0.2007	0.1998	0.1997	0.2001	3.35e−06	0.60e−06	0.20e−06	0.15e−07
β_2	0.1500	0.1504	0.1503	0.1499	3.76e−06	0.78e−06	0.23e−06	0.20e−07
β_3	0.1988	0.1999	0.2003	0.2000	4.48e−06	0.77e−06	0.26e−06	0.24e−07
β_4	0.3622	0.3814	0.3663	0.3718	1.788	0.191	0.075	0.007

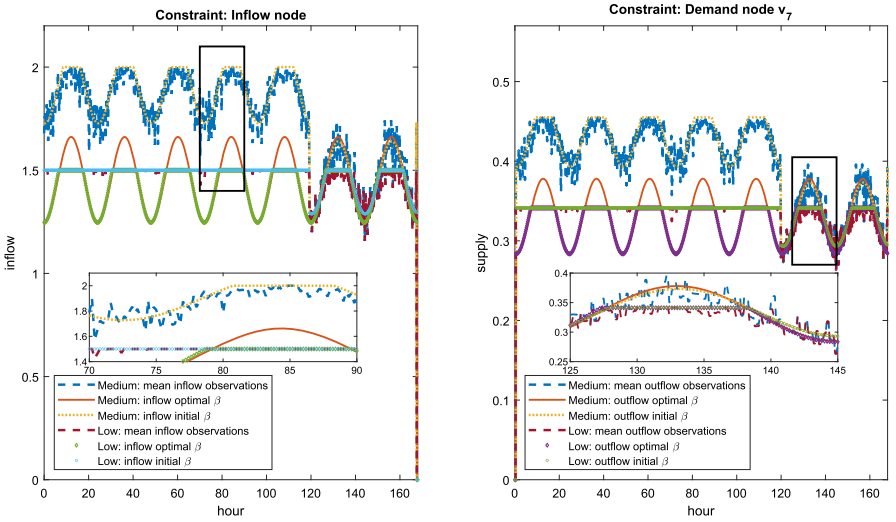

Fig. 14 A comparison between the mean realization of the $p = 6$ historical in- and outflows with the in- and outflow for the reconstructed β in the case of Sect. 3.3.4 and the initial β where observations can only be made on Sundays ($t \in [144, 168]$) with two different inflow constraints

Under additional inflow constraints, Fig. 14 shows the behavior of the in- and outflows according to the choices for the initial and reconstructed β. For the medium inflow constraint of level 2, we observe that from Monday to Friday the reconstructed in- and outflow deviate significantly from the outflow observations, since all the measurements were taken on Sunday. This is also underlined by Table 8 where, in this case, we find a highly varying reconstructed β_4, depicting that the choice of β_4 cannot be controlled and has no impact on the objective function. During the weekend, the observed outflow and the outflow from the optimally reconstructed β are in good agreement. This is no longer true when considering the lower constraint where the inflow is also cut on Sundays. Therefore, as in all previous examples, the reconstruction of β is not successful for the low inflow constraint.

Table 8 Means and variances of the reobtained weights for the base demands for different choices of the number of perturbed historical observations p with observations only for $t \in [144, 168]$ from Sect. 3.3.4 with additional inflow constraints

	mean				variance			
	medium		low		medium		low	
	$p = 6$	$p = 200$	$p = 6$	$p = 200$	$p = 6$	$p = 200$	$p = 6$	$p = 200$
β_1	0.1763	0.1760	0.2192	0.2443	0.56e−04	0.16e−05	0.465e−04	0.343e−06
β_2	0.1665	0.1684	0.1206	0.0966	0.78e−04	0.31e−05	0.481e−04	0.390e−06
β_3	0.2220	0.2240	0.1642	0.1377	0.86e−04	0.22e−05	0.574e−04	0.571e−06
β_4	0.3452	0.3578	0.3001	0.3133	0.1934	0.009	0.215	0.013

4 Conclusions

The present paper is devoted to the inverse demand tracking over transportation networks of tree shape governed by linear hyperbolic conservation laws. By considering this problem in the setting of Lebesgue spaces for control variables, we were in position to ensure the existence of optimal solutions. These were numerically computed by solving an associated finite-dimensional nonsmooth optimization problem which results from the original hierarchical model by plugging the pointwise computable Lipschitzian solution operator of the subordinate convex network flow problem into the upper-level objective function before discretizing the resulting single-level problem by means of a finite differences scheme. Numerical experiments demonstrated that for full time observation operators in the absence of control constraints, there is a very good agreement of solutions for the optimal and the benchmark problem. Restricted-in-time observation operators or the presence of control constraints may lead to different solutions, depending on the choice of the underlying base demands or the restrictiveness of the employed constraint.

Our findings give rise to at least two interesting directions for future research. First, it is well known that several network dynamics obey nonlinear hyperbolic partial differential equations like the flow of gases, see e.g. Bressan (2000), while, in this paper, we focused on merely linear dynamics. We note that incorporating nonlinear dynamics in an inverse optimal control problem makes the lower-level problem nonconvex and, thus, an explicit computation of the lower-level solution operator is highly challenging, see Remark 2.8 as well. Furthermore, one cannot simply replace the lower-level problem by (necessary but not necessarily sufficient) optimality conditions without enlarging the feasible set significantly. Second, in the setting discussed in this paper, it might be worth trying to solve the finite-dimensional nonsmooth single-level problem with a more enhanced numerical scheme than just MATLAB's `patternsearch` method. Indeed, the special structure of the Lipschitzian lower-level solution operator discussed in Appendix A allows for an explicit computation of its so-called Clarke generalized Jacobian, see (Clarke 1983), and this object can be used to construct a bundle-type algorithm, see (Schramm and Zowe 1992), for the numerical solution of the nonsmooth optimization problem of interest since the latter merely possesses

affine constraints, see the classical paper (Dempe and Bard 1992) for a related idea and Gfrerer and Outrata (2024) for a modern view.

A Special quadratic problems with box constraints

Let us fix vectors $\theta, v_\mathrm{d} \in \mathbb{R}^n$ as well as $v_\mathrm{a} \in (\mathbb{R} \cup \{-\infty\})^n$ and $v_\mathrm{b} \in (\mathbb{R} \cup \{\infty\})^n$ such that all entries of θ are positive while $v_\mathrm{a} \leq v_\mathrm{b}$ holds componentwise. For $\Theta := \mathrm{diag}(\theta)$, we aim to solve

$$\min_v \{\tfrac{1}{2} v^\top \Theta v - v_\mathrm{d}^\top v \mid v \in V_\mathrm{ad}\} \tag{QP}$$

where $V_\mathrm{ad} \subset \mathbb{R}^n$ is the box given by

$$V_\mathrm{ad} := \{v \in \mathbb{R}^n \mid v_\mathrm{a} \leq v \leq v_\mathrm{b}\}.$$

First, we observe that the objective function in (QP) is uniformly convex while the feasible set is nonempty, closed, and convex. Hence, (QP) possesses a uniquely determined global minimizer $\bar{v} \in V_\mathrm{ad}$. The latter can be characterized in terms of the necessary and sufficient optimality condition

$$\forall v \in V_\mathrm{ad}: \quad (\Theta \bar{v} - v_\mathrm{d})^\top (v - \bar{v}) \geq 0. \tag{A.1}$$

We note that Θ is a positive definite diagonal matrix. Hence, it is reasonable to set

$$\tilde{v} := \Theta^{-1} v_\mathrm{d}.$$

Note that $\tilde{v}_i = \theta_i^{-1} v_{\mathrm{d},i}$ holds for all $i = 1, \ldots, n$. We will now show that

$$\bar{v} = \max(v_\mathrm{a}, \min(\tilde{v}, v_\mathrm{b})) \tag{A.2}$$

holds true, i.e., that $\bar{v}$ is the projection of $\tilde{v}$ onto the box V_ad. Note that max and min have to be interpreted componentwise in (A.2). We introduce index sets $I_\mathrm{a}, I_0, I_\mathrm{b} \subset \{1, \ldots, n\}$ by means of

$$\begin{aligned} I_\mathrm{a} &:= \{i \in \{1, \ldots, n\} \mid \tilde{v}_i < v_{\mathrm{a},i}\}, \\ I_0 &:= \{i \in \{1, \ldots, n\} \mid v_{\mathrm{a},i} \leq \tilde{v}_i \leq v_{\mathrm{b},i}\}, \\ I_\mathrm{a} &:= \{i \in \{1, \ldots, n\} \mid v_{\mathrm{b},i} < \tilde{v}_i\}. \end{aligned}$$

Clearly, these sets form a disjoint partition of $\{1, \ldots, n\}$, and (A.2) can be rewritten as

$$\forall i \in \{1, \ldots, n\}: \quad \bar{v}_i = \begin{cases} v_{\mathrm{a},i} & i \in I_\mathrm{a}, \\ \tilde{v}_i & i \in I_0, \\ v_{\mathrm{b},i} & i \in I_\mathrm{b}. \end{cases}$$

Pick $v \in V_{\mathrm{ad}}$ arbitrarily. Taking together all of the above findings, we end up with

$$
\begin{aligned}
&(\Theta\bar{v} - v_{\mathrm{d}})^{\top}(v - \bar{v}) \\
&\quad = \sum_{i \in I_{\mathrm{a}}} (\theta_i v_{\mathrm{a},i} - v_{\mathrm{d},i}) \underbrace{(v_i - v_{\mathrm{a},i})}_{\geq 0} + \sum_{i \in I_{\mathrm{b}}} (\theta_i v_{\mathrm{b},i} - v_{\mathrm{d},i}) \underbrace{(v_i - v_{\mathrm{b},i})}_{\leq 0} + \sum_{i \in I_0} \underbrace{(\theta_i \tilde{v}_i - v_{\mathrm{d},i})}_{=0} (v_i - \tilde{v}_i) \\
&\quad \geq \sum_{i \in I_{\mathrm{a}}} \underbrace{(\theta_i \tilde{v}_i - v_{\mathrm{d},i})}_{=0} (v_i - v_{\mathrm{a},i}) + \sum_{i \in I_{\mathrm{b}}} \underbrace{(\theta_i \tilde{v}_i - v_{\mathrm{d},i})}_{=0} (v_i - v_{\mathrm{b},i}) = 0,
\end{aligned}
$$

and this shows that $\bar{v}$ constructed as in (A.2) is, indeed, a solution of (A.1) and, thus, the uniquely determined global minimizer of (QP).

Acknowledgements The authors wish to thank the two anonymous reviewers whose valuable comments and suggestions helped to improve the overall quality of this paper. Furthermore, one of the reviewers recommended an inspection of the PhD thesis (Keimer 2014) which is gratefully acknowledged. Simone Göttlich was supported by the Deutsche Forschungsgemeinschaft (DFG) within the projects GO1920/10-1 and GO1920/11-1.

Funding Open Access funding enabled and organized by Projekt DEAL.

Declarations

Conflict of interest The authors declare no Conflict of interest.

References

Albrecht S, Ulbrich M (2017) Mathematical programs with complementarity constraints in the context of inverse optimal control for locomotion. Optim Methods Softw 32(4):670–698. https://doi.org/10.1080/10556788.2016.1225212

Albrecht S, Passenberg C, Sobotka M, Peer A, Buss M, Ulbrich M (2010) Optimization criteria for human trajectory formation in dynamic virtual environments. In: Kappers AML, van Erp JBL, Bergmann Tiest WM, van der Helm FDT (eds) Haptics: generating and perceiving tangible sensations. Springer, Berlin, pp 257–262. https://doi.org/10.1007/978-3-642-14075-4_37

Albrecht S, Leibold M, Ulbrich M (2012) A bilevel optimization approach to obtain optimal cost functions for human arm movements. Numer Algebra Control Optim 2(1):105–127. https://doi.org/10.3934/naco.2012.2.105

Banda MK, Herty M, Klar A (2006) Gas flow in pipeline networks. Netw Heterog Media 1(1):41–56. https://doi.org/10.3934/nhm.2006.1.41

Bard JF (1998) Practical bilevel optimization. Springer, New York. https://doi.org/10.1007/978-1-4757-2836-1

Bressan A (2000) Hyperbolic systems of conservation laws-the one-dimensional cauchy problem. Oxford University Press, Oxford. https://doi.org/10.1093/oso/9780198507000.001.0001

Bressan A, Čanić S, Garavello M, Herty M, Piccoli B (2014) Flows on networks: recent results and perspectives. EMS Surv Math Sci 1(1):47–111. https://doi.org/10.4171/EMSS/2

Clarke FH (1983) Optimization and nonsmooth analysis. Wiley, New York. https://doi.org/10.1137/1.9781611971309

Colton D, Kress R (2013) Inverse acoustic and electromagnetic scattering theory. Springer, New York. https://doi.org/10.1007/978-1-4614-4942-3

Coskun S, Korn R (2021) Modeling the intraday electricity demand in Germany. In: Göttlich S, Herty M, Milde A (eds) Mathematical modeling, simulation and optimization for power engineering and management. Springer, Cham, pp 3–23. https://doi.org/10.1007/978-3-030-62732-4_1

Dempe S (2002) Foundations of bilevel programming. Kluwer, Dordrecht. https://doi.org/10.1007/b101970

Dempe S (2020) Bilevel optimization: theory, algorithms, applications and a bibliography. In: Dempe S, Zemkoho AB (eds) Bilevel optimization: advances and next challenges. Springer, Cham, pp 581–672. https://doi.org/10.1007/978-3-030-52119-6_20

Dempe S, Bard JF (1992) Bundle trust-region algorithm for bilinear bilevel programming. J Optim Theory Appl 110:265–288. https://doi.org/10.1023/A:1017571111854

Dempe S, Kalashnikov V, Pérez-Valdéz G, Kalashnykova N (2015) Bilevel programming problems-theory, algorithms and applications to energy networks. Springer, Berlin. https://doi.org/10.1007/978-3-662-45827-3

Dempe S, Harder F, Mehlitz P, Wachsmuth G (2019) Solving inverse optimal control problems via value functions to global optimality. J Global Optim 74(2):297–325. https://doi.org/10.1007/s10898-019-00758-1

Dobrowolski M (2006) Angewandte Funktionalanalysis. Springer, Berlin. https://doi.org/10.1007/3-540-29960-2

Friedemann M, Harder F, Wachsmuth G (2023) Finding global solutions of some inverse optimal control problems using penalization and semismooth Newton methods. J Global Optim 86:1025–1061. https://doi.org/10.1007/s10898-023-01288-7

Gfrerer H, Outrata JV (2024) On the role of of semismoothness in nonsmooth numerical analysis: theory. https://arxiv.org/abs/2405.14637

Göttlich S, Schillinger T (2022a) Control strategies for transport networks under demand uncertainty. Adv Comput Math 48:74. https://doi.org/10.1007/s10444-022-09993-9

Göttlich, S, Schillinger T (2022b) Stochastic optimal control for nonlinear damped network dynamics. arXiv:2202.05114

Göttlich S, Herty M, Schillen P (2016) Electric transmission lines: control and numerical discretization. Optimal Control Appl Methods 37(5):980–995. https://doi.org/10.1002/oca.2219

Göttlich S, Korn R, Lux K (2019) Optimal control of electricity input given an uncertain demand. Math Methods Oper Res 90:301–328. https://doi.org/10.1007/s00186-019-00678-6

Gugat M, Keimer A, Leugering G, Wang Z (2015) Analysis of a system of nonlocal conservation laws for multi-commodity flow on networks. Netw Heterog Media 10(4):749–785. https://doi.org/10.3934/nhm.2015.10.749

Gugat M, Schultz R, Wintergerst D (2018) Networks of pipelines for gas with nonconstant compressibility factor: stationary states. Comput Appl Math 37(2):1066–1097. https://doi.org/10.1007/s40314-016-0383-z

Harder F, Wachsmuth G (2019) Optimality conditions for a class of inverse optimal control problems with partial differential equations. Optimization 68(2–3):615–643. https://doi.org/10.1080/02331934.2018.1495205

Hatz K, Schlöder JP, Bock HG (2012) Estimating parameters in optimal control problems. SIAM J Sci Comput 34(3):A1707–A1728. https://doi.org/10.1137/110823390

Hinze M, Pinnau R, Ulbrich M, Ulbrich S (2009) Optimization with PDE constraints. Springer, Dordrecht. https://doi.org/10.1007/978-1-4020-8839-1

Holler G, Kunisch K, Barnard RC (2018) A bilevel approach for parameter learning in inverse problems. Inverse Prob 34(11):1–28. https://doi.org/10.1088/1361-6420/aade77

Keimer A (2014) Optimal control of nonlinear nonlocal conservation laws on networks. PhD thesis, University of Erlangen–Nuremberg. https://open.fau.de/items/b9a127b7-0e85-43d0-822b-f391b6f206ea

Mehlitz P, Wachsmuth G (2020) Bilevel optimal control: existence results and stationarity conditions. In: Dempe S, Zemkoho AB (eds) Bilevel optimization: advances and next challenges. Springer, Cham, pp 451–484. https://doi.org/10.1007/978-3-030-52119-6_16

Mombaur K, Truong A, Laumond J-P (2010) From human to humanoid locomotion–an inverse optimal control approach. Auton Robot 28(3):369–383. https://doi.org/10.1007/s10514-009-9170-7

Rein M, Mohring J, Damm T, Klar A (2020) Optimal control of district heating networks using a reduced order model. Optimal Control Appl Methods 41(4):1352–1370. https://doi.org/10.1002/oca.2610

Schramm H, Zowe J (1992) A version of the bundle idea for minimizing a nonsmooth function: conceptual idea, convergence analysis, numerical results. SIAM J Optim 2(1):121–152. https://doi.org/10.1137/0802008

Shimizu K, Ishizuka Y, Bard JF (1997) Nondifferentiable and two-level mathematical programming. Springer, New York. https://doi.org/10.1007/978-1-4615-6305-1

Sikolya E (2004) Semigroups for flows in networks. PhD thesis, University of Tübingen. https://d-nb.info/972906657/34

Suryan V, Sinha A, Malo P, Deb K (2016) Handling inverse optimal control problems using evolutionary bilevel optimization. In: 2016 IEEE congress on evolutionary computation (CEC), pp 1893–1900. https://doi.org/10.1109/CEC.2016.7744019

Tröltzsch F (2010) Optimal control of partial differential equations. Am Math Soc. https://doi.org/10.1090/gsm/112

Troutman JL (1996) Variational calculus and optimal control. Springer, New York. https://doi.org/10.1007/978-1-4612-0737-5

Vinter R (2010) Optimal control. Birkhäuser, Boston. https://doi.org/10.1007/978-0-8176-8086-2

Zemkoho AB (2016) Solving ill-posed bilevel programs. Set-Valued Var Anal 24:423–448. https://doi.org/10.1007/s11228-016-0371-x